IEEE Access
Multidisciplinary ⋮ Rapid Review ⋮ Open Access Journal

Received 15 May 2023, accepted 1 June 2023, date of publication 6 June 2023, date of current version 15 June 2023.

Digital Object Identifier 10.1109/ACCESS.2023.3283293

RESEARCH ARTICLE

Physical Layer Security of Dual-Hop Hybrid FSO-mmWave Systems

SAUD ALTHUNIBAT[1], (Senior Member, IEEE), SEZER C. TOKGOZ[2], (Member, IEEE), SERHAN YARKAN[3], (Senior Member, IEEE), SCOTT L. MILLER[4], AND KHALID A. QARAQE[5], (Senior Member, IEEE)

[1]Department of Communication Engineering, Al-Hussein Bin Talal University, Ma'an 71111, Jordan
[2]WR&D, Qualcomm Technologies Inc., San Diego, CA 92121, USA
[3]Department of Electrical and Electronics Engineering, Istanbul Commerce University, 34840 Istanbul, Turkey
[4]Department of Electrical and Computer Engineering, Texas A&M University, College Station, TX 77843, USA
[5]Department of Electrical and Computer Engineering, Texas A&M University at Qatar, Doha, Qatar

Corresponding author: Saud Althunibat (saud.althunibat@ahu.edu.jo)

This publication was made possible by NPRP13S-0130-200200 from the Qatar National Research Fund (a member of The Qatar Foundation). The statements made herein are solely the responsibility of the author[s].

ABSTRACT Hybrid free-space optical (FSO) and millimeter wave (mmWave) systems have been proposed as an efficient solution to improve spectral efficiency and maintain link reliability. The comparable supported data rate and the complementary characteristics in different weather conditions of both links, i.e., FSO and mmWave) have attracted research efforts towards analyzing the different performance aspects of hybrid FSO-mmWave systems. Following this direction, in this article, the physical-layer security analysis of the dual-hop hybrid FSO-mmWave systems is addressed. In the considered system, both FSO and mmWave links are simultaneously used to carry data at each hop, while an eavesdropper is assumed to present to wiretap either one or both links. The analysis includes building a mathematical framework to derive different secrecy metrics, such as the average secrecy capacity, secrecy outage probability and effective secrecy throughput metrics, in mathematical expressions. Obtained analytical results are verified using Monte Carlo simulations where exact matching are achieved. Moreover, the presented results include investigation of the impact of the different operational parameters on the overall secrecy performance.

INDEX TERMS Physical layer security, cooperative systems, relaying schemes, free space optical, millimeter wave band, hybrid FSO-mmWave, secrecy analysis.

I. INTRODUCTION

Recently, research efforts are being directed to exploit hgigh frequency bands to meet 5G requirements represented by unexpected volumes of data exchange along with scare radio frequency (RF) resources. Compared to 4G, required data volumes are estimated to be at least a thousand fold greater [1], [2], [3], [4]. Compared to the congested RF, Free-space optical (FSO) communication has been widely nominated as a candidate for future wireless systems due to its low energy expenditure, immunity to interference, and acceptable level of security [5]. However, FSO technology still suffers from some challenges which include sensitivity to line-of-sight (LOS) alignments and poor performance under different weather conditions such as thermal expansion, wind load, and foggy weather [6], [7]. On the other hand, recent studies on millimeter waves (*mm*Wave) bands have demonstrated that multi-gigabit data rates can be attained along with different impact of the weather conditions on *mm*Wave [8]. Specifically, the impact of thermal expansion, wind and fog on *mm*Wave band is considered trivial, while it is highly affected by oxygen absorption and rain. Also, compared to FSO, energy consumption and attack vulnerability in *mm*Wave are considered serious challenges. To this end, the above reported complementary properties of both FSO and *mm*Wave have motivated recent research works toward hybrid links of FSO and *mm*Wave to strike a balance between data rate, security and reliability [9], [10], [11],

The associate editor coordinating the review of this manuscript and approving it for publication was Adao Silva.

[12], [13]. Notice that the achievable data rates of both technologies are comparable, which in turn, paves the way for the FSO*mm*Wave parallel utilization aiming at transmit diversity improvement, spectral efficiency enhancement and/or security level boosting [14], [15], [16]. In another perspective, relaying schemes are widely used as an energy efficient technique, to increase the coverage area and system reliability as well as the system capacity [17], [18], [19]. Therefore, considering high demands/requirements of 5G and beyond era, relay-based methods have been extensively employed utilizing hybrid combinations of both FSO and *mm*Wave in which the signal is first transmitted from the source over either FSO or *mm*Wave link, and forwarded by a relay node using different link (either FSO or *mm*Wave) towards the destination node. Such a relying system has shown a promising performance compared to traditional relaying schemes [13].

A. RELATED WORKS

As mentioned earlier, literature works in hybrid FSO/RF based relaying systems have recently shown an increasing interest. For instance, different performance aspects of hybrid and/or dual-hop systems are deeply analyzed in [20], [21], [22], [23], [24], [25], [26], and [27] taking into account different system operation parameters such as fixed- and variable-gain amplift-and-forward (AF) relaying schemes based on multiple scenarios and assumptions. The authors in [28], [29], [30], and [31] address the relay selection of a set of AF relays for mixed FSO/RF systems based on outdated channel state information. It is based on the assumption that RF link is subject to Rayleigh fading while the FSO link is impacted by Gamma-Gamma atmospheric turbulence. Further, generalized performance analyses of mixed FSO-RF systems is in detail examined in [32], [33], [34], and [35] considering multi-hop transmissions, in which the effect of co-channel interference at both relay and destination, threshold-based selective switching schemes, higher order moments, fading, and moment generating function are considered. In the works [36], [37], [38], multiuser dual-hop relaying systems over mixed RF and FSO links are investigated with opportunistic user scheduling, where links between the users and the relay are operating on RF band, while the link between the relay and the destination is operating on an FSO link. Alternatively, secrecy analysis of a mixed RF-FSO dual-hop system in the presence of a single eavesdropper is conducted in [39], [40], [41], [42], [43], and [44]. It is assumed that the eavesdropper is wire-taping the RF link only, and both fixed- and variable-gain relaying are considered. Their studies result in analytical expression for the average secrecy capacity (ASC) and the secrecy outage probability (SOP). In a different scenario, ASC and SOP of a mixed single-input multiple-output simultaneous wireless information and power transfer based RF and FSO system are addressed in [45] and [46]. The eavesdropper is assumed to be an energy harvesting RF receiver. The study yields in analytical formulas of both ASC and SOP considering different detection methods and the impact of pointing errors in FSO. In [47], the performance of secrecy capacity of a satellite-to-terrestrial multi-hop system is assessed, where RF is adopted for the satellite link while the terrestrial link is operated by FSO. Accurate mathematical expressions for both the ASC and SOP are derived considering AF and decode-and-forward (DF) relaying techniques while the eavesdropper can wiretap to satellite link only. The secrecy outage probability of a hybrid RF-FSO scheme is investigated assuming imperfect channel estimation process in [48], [49], and [50], where a multi-antenna eavesdropper is considered for a SIMO system. Also in [51], a multi-antenna eavesdropper is assumed to be present in a MIMO based relaying system. The secrecy analysis is conducted considering different selection mechanisms of the transmit antennas.

B. MOTIVATION AND CONTRIBUTIONS

Early discussed works [21], [22], [23], [24], [25], [26], [27], [28], [29], [30], [31], [32], [33], [34], [35], [36], [37], [38], [39], [40], [41], [42], [43], [44], [45], [46], [47], [48], [49], [50], [51], [52] have addressed the performance aspects of mixed, dual-hop, and/or relaying schemes for FSO and RF systems considering different scenarios and assumptions. In all considered scenarios, either RF or FSO is employed alone in one of the hops. However, as mentioned earlier, the performance of dual-hop mixed relaying systems are dramatically degraded in some weather conditions. Therefore, employing parallel combinations in which simultaneous transmissions over both FSO and RF links in the same hop has been proposed as an efficient solution to maintain the reliability of relaying systems in different weather conditions. Moreover, traditional RF-only back-haul links are not sufficient for the recent requirements including extreme reliability, low latency, and high capacity, which enables the need for hybrid systems. Consequently, one hop hybrid FSO-RF systems are investigated in [53], [54], [55], [56], [57], and [58] considering various configurations. Afterwards, the authors in [59], [60], [61], [62], and [63] examine relay-based hybrid FSO and RF systems for connecting macro-cell base station with small-cell base station through multiple parallel buffer-aided relay nodes, optimal fixed and adaptive link allocation policies to share the transmission time, and link selection in each hop. In [64], the outage probability of the hybrid FSO-*mm*Wave system is investigated, while the PLS analysis of direct link (single hop) hybrid FSO-*mm*Wave systems is investigated considering uncorrelated links in [65] and correlated links in [66].

Motivated by the above, in this paper, we consider hybrid FSO-*mm*Wave dual-hop systems, where both FSO and *mm*Wave are simultaneously utilized in each hop, for further analysis and investigation. In particular, we examine the secrecy capacity of the two well-known AF relaying schemes, namely, fixed-gain (FG) and variable-gain (VG) AF relaying schemes. Recall that FG and VG imply that power amplification at the AF relay is conducted based on partial or perfect channel information, respectively.

It is worth highlighting that despite the fact that the utilization of hybrid FSO-RF systems is a promising remedy for future back-haul links, physical layer security analysis of dual-hop hybrid FSO-RF systems has not yet been investigated to the best of our knowledge. Therefore, for the first time, the secrecy performance of a hybrid FSO-RF system is investigated considering two well-known AF relaying schemes, namely, variable- and fixed-gain schemes. Three different types of eavesdroppers are considered, namely, RF-, FSO- and Hybrid-Eve, with a relevant secrecy performance comparison. Also, more practical conditions are assumed represented by Gamma-Gamma atmospheric turbulence and Nakagami-*m* fading for FSO and RF links, respectively. Our results include analyzing different performance metrics, which results in novel analytical expressions for the secrecy capacity, secrecy outage probability and effective throughout for fixed-gain and variable-gain AF relaying methods. Moreover, in order to validate the analytical accuracy of the proposed derivations, Monte-Carlo simulations are presented along with related theoretical results considering several fundamental physical layer parameters. The contributions of this paper can be summarized as follows:

- Investigating the secrecy performance of dual-hop hybrid FSO-*mm*Wave systems by evaluating the secrecy capacity.
- Deriving mathematical expressions for the secrecy capacity considering two different AF relaying schemes, variable- and fixed-gain relaying.
- Considering three different types of potential eavesdroppers that can wiretap either FSO link, *mm*Wave link or both links.
- Analysing the performance by a set of simulation and analytical results while considering the different weather conditions, eavesdropper types and relaying schemes.

C. PAPER ORGANIZATION

The organization of the rest of the paper is as follows: Section II describes the system and channel models for hybrid FSO-*mm*Wave communications. SNR models of fixed- and variable-gain AF relaying schemes are presented in Section III. The secrecy analysis of dual-hop hybrid FSO-*mm*Wave system is presented in Section IV for AF relaying schemes. The results are given in Section V along with relevant discussions. Finally, Section VI concludes the paper.

II. SYSTEM MODEL

We consider a dual-hop hybrid FSO-*mm*Wave system, where the classic Wyner's wiretap channels take place [67]. The legitimate transmitter, Alice, wants to send a confidential information to the legitimate receiver, Bob, by the aid of a relay node. An eavesdropper, Eve, is assumed present and is trying to wiretap on the legitimate communication by sniffing the received signals at the Bob's side, as illustrated in Fig. 1. In each hop, i.e., the first-hop (from Alice to relay) and the second-hop (from relay to Bob), two parallel links, namely, an FSO link and an RF link are activated for data transmission. Accordingly, for the data transmission over the RF link, it is assumed that Alice and Bob are equipped by a single transmit antenna and a single receive antenna, respectively, while the relay node is equipped by a single transmit antenna and a single receive antenna. For the FSO link, Alice utilizes a single laser, while Bob utilizes a single photodetector. The relay node is equipped by a single photodetector and a single laser for reception and transmission ove the FSO link. At the relay node, two well-known AF relaying schemes are considered in both hops,namely, FG and VG AF relaying methods. In FG AF relying, the power amplification is determined based on partial channel information, while in VG AF, the full channel state info is adopted to determine the power amplification level. Data flow at Alice is split into symbols, each of $\log_2(M)$ bits, where M denotes the modulation order. As both links are activated, each symbol, after being modulated, will be transmitted over each link. As RF is operated over the *mm*Wave band, it is assumed that both links provide identical bandwidth.

In this work, Eve is considered to be one of three types according to its ability and resources. The first type is RF-Eve which is able to wiretap the RF link only, while the second is FSO-Eve that wiretaps the FSO link only. Differently, Hybrid-Eve is able to wiretap both links using a single receive antenna and a single photodetector.

It is worthy to note that through this study, the subscript $x \in \{1, 2, b, e\}$ denotes either hop number or receiving side, i.e., $x = 1$ for the first-hop, $x = 2$ is for the second-hop, $x = b$ for legitimate receiver Bob, and $x = e$ for the eavesdropper Eve.

A. FREE-SPACE OPTICAL (FSO) SUBSYSTEM

1) CHANNEL CHARACTERISTIC

Among the different models to describe the irradiance of the received optical signal ini FSO link, the well-known Gamma-Gamma turbulence model has been widely adopted in the literature. This is mainly due to its doubly stochastic scintillation model. Specifically, the received intensity is modeled as the product of two independent Gamma random variables (RVs) which represent the irradiance fluctuations caused by large- and small-scale atmospheric-turbulence [5], [68], [69]. In our study, the RV I is adopted to represent the instantaneous irradiance which follows a Gamma-Gamma distribution. The related probability density function (PDF) is given as [68, (57)]

$$f_I(i) = \frac{2(\alpha\beta)^{(\alpha+\beta)/2}}{\Gamma(\alpha)\Gamma(\beta)} i^{\frac{\alpha+\beta}{2}-1} K_{\alpha-\beta}(2\sqrt{\alpha\beta i}), \tag{1}$$

where $i \geq 1$, $K_\nu(\cdot)$ represents the modified Bessel function of the second kind of the ν^{th} order, and $\Gamma(\cdot)$ depicts the Gamma function. The parameters α and β represent the small-scale and large-scale coefficients, respectively, which

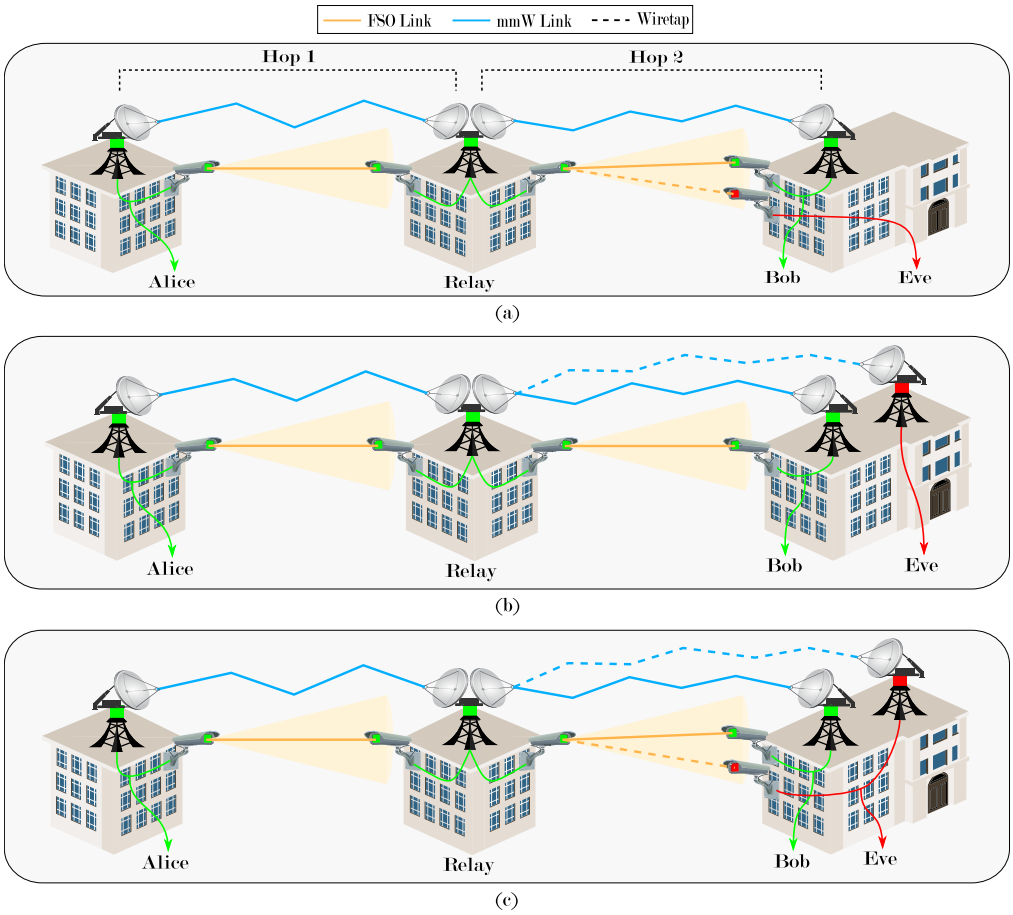

FIGURE 1. System model of a dual hop hybrid FSO-*mm*Wave communications between the legitimate transmitter Alice and receiver Bob in the presence of different type eavesdroppers: (a)FSO-Eve, (b) RF-Eve, and (c)-Hybrid-Eve.

can be obtained as [68, (58)-(59)]

$$\alpha = \exp\left\{\exp\left[\frac{0.49\zeta^2}{\left(1+0.65\vartheta^2+1.11\zeta^{12/5}\right)^{7/6}}\right]-1\right\}^{-1}, \tag{2}$$

$$\beta = \exp\left\{\exp\left[\frac{0.51\zeta^2\left(1+0.69\zeta^{12/5}\right)^{-5/6}}{1+0.9\vartheta^2+0.62\vartheta^2\zeta^{12/5}}\right]-1\right\}^{-1}, \tag{3}$$

where $\zeta^2 = 1.23C_n^2\Lambda^{7/6}d^{11/6}$ is the Rytov variance, and $\vartheta = \sqrt{\Lambda A^2/4d}$. Here, $\Lambda = 2\pi/\lambda_o$ is the optical wave number, λ_o is the wavelength (optical carrier), d is the link distance, A is the diameter of the lens aperture at the receiver photodetector, and C_n^2, defined by the Hufnagel-Valley (HV5/7) model [69], denotes the weather-altitude depended refractive index.

2) SIGNAL-TO-NOISE RATIO MODEL

The instantaneous electrical signal-to-noise ratio (SNR) at the output of FSO receiving photodetector, $\gamma_{x,o}$, is expressed as

$$\gamma_{x,o} = \overline{\gamma}_{x,o} I_x^2, \tag{4}$$

where I_x represents the normalized irradiance turbulence, and $\overline{\gamma}_{x,o}$ is the average electrical SNR of the FSO link, given as

$$\overline{\gamma}_{x,o} = \left(\frac{\eta I_t R_{x,o} L_{x,o}}{\sigma_x}\right)^2, \tag{5}$$

η denotes the optical-to-electrical conversion efficiency, I_t stands for the radiant emittance of the laser from Alice, $R_{x,o}$ depicts the fraction of captured light intensity ($R_{x,o} \in [0, 1)$), and $L_{x,o}$ denotes the path loss affected the optical intensity given as

$$L_{x,o} = \frac{\pi A^2}{4(\psi d_x)^2}\exp\left[-\varphi_o d_x\right], \tag{6}$$

where ψ represents the beam divergence of the laser, φ_o denotes the attenuation extinction coefficient, and d_x represents the distance between Alice and the receiving side. Accordingly, the PDF of the electrical SNR can be obtained by transformation of the RV I in (1) to yeild:

$$f_{\gamma_o}(\gamma_{x,o}) = \frac{(\alpha_x\beta_x)^{\frac{(\alpha_x+\beta_x)}{2}}}{\Gamma(\alpha_x)\Gamma(\beta_x)\overline{\gamma}_{x,o}^{\frac{\alpha_x+\beta_x}{4}}}\gamma_{x,o}^{\frac{\alpha_x+\beta_x}{4}-1}$$

$$\times G_{0,2}^{2,0}\left(\frac{\alpha_x\beta_x}{\sqrt{\overline{\gamma}_{x,o}}}\sqrt{\gamma_{x,o}}\middle|\begin{matrix}-,-\\ \frac{\alpha_x-\beta_x}{2},\frac{\alpha_x-\beta_x}{2}\end{matrix}\right), \quad (7)$$

accordingly, the cumulative density function (CDF) of SNR can be obtained as

$$F_{\gamma_o}(\gamma_{x,o}) = \frac{1}{\Gamma(\alpha_x)\Gamma(\beta_x)} G_{1,3}^{2,1}\left(\frac{\alpha_x\beta_x}{\sqrt{\overline{\gamma}_{x,o}}}\sqrt{\gamma_{x,o}}\middle|\begin{matrix}1\\ \alpha_x,\beta_x,0\end{matrix}\right). \quad (8)$$

B. MILLIMETER WAVE (mmWave) SUBSYSTEM

1) CHANNEL CHARACTERISTIC

Unlike the traditional RF in the lower bands, the channel statistics of the *mm*Wave band has not been widely investigated. Most of the literature in *mm*Wave band focuses on the large-scale propagation effects [70], [71], [72], while the smal-scale fading in *mm*Wave band is shown to be mathematically intractable according to the 5G standard prepared by 3GPP organization [73]. However, Nakagami-*m* fading model is widely used in the literature to express the channel fading in *mm*Wave [74]. Therefore, the RV H, denoting the instantaneous channel coefficent in the *mm*Wave band, is assumed to follow Nakagami-*m* distribution whose PDF is given as

$$f_H(h) = \frac{2m^m}{\Gamma(m)} h^{2m-1} e^{-mh^2}, \quad (9)$$

where m denotes the fading order/severity.

2) SIGNAL-TO-NOISE RATIO

The instantaneous electrical SNR at the output of *mm*Wave receiving antenna, $\gamma_{x,f}$, is expressed as

$$\gamma_{x,f} = \overline{\gamma}_{x,f} H_x^2, \quad (10)$$

where H_x depicts the instantaneous channel gain, and $\overline{\gamma}_{x,f}$ is the average electrical SNR of the RF link, given as

$$\overline{\gamma}_{x,f} = \frac{P_t R_{x,f} L_{x,f}}{\sigma_x^2}, \quad (11)$$

where P_t denotes the transmit power from Alice, $R_{x,f} \in [0, 1)$ stands for the fraction of received power, and $L_{x,f}$ represents the path loss between Alice and the receiving side, which is given as [74]

$$L_{x,f} = \frac{G_T G_R \lambda_f^2}{(4\pi d_x)^2 (\varphi_{O_2} d_x)(\varphi_f d_x)}, \quad (12)$$

where G_T and G_R, in turn, are the gains of transmitting and receiving antennas, λ_f denotes the RF carrier wavelength, and φ_{O_2} and φ_f stands for the attenuation coefficients caused by the oxygen absorption and rainy weather condition, respectively. It is well-known, based on (9), the instantaneous SNR over Nakagami-*m* fading channel distributed according to a Gamma distribution expressed as [75, (2.21)]

$$f_{\gamma_f}(\gamma_{x,f}) = \frac{m_x^{m_x}}{\Gamma(m_x)\overline{\gamma}_{x,f}^{m_x}} \gamma_{x,f}^{m_x-1} \exp\left[-\frac{m_x}{\overline{\gamma}_{x,f}}\gamma_{x,f}\right], \quad (13)$$

accordingly, the CDF of SNR can be obtained as

$$F_{\gamma_f}(\gamma_{x,f}) = \frac{1}{\Gamma(m_x)} \Gamma_L\left(m_x, \frac{m_x\gamma_{x,f}}{\overline{\gamma}_{x,f}}\right), \quad (14)$$

where $\Gamma_L(\cdot,\cdot)$ represent the lower incomplete Gamma function, and alternatively, the CDF of SNR can be re-expressed as [76, Eq. 8.352.1]

$$\begin{aligned} F_{\gamma_f}(\gamma_{x,f}) &= \frac{(m_x-1)!}{\Gamma(m_x)} \\ &\quad \times \left[1 - \exp\left(\frac{m_x}{\overline{\gamma}_{x,f}}\gamma_{x,f}\right) \sum_{k=0}^{m_x-1} \frac{\left(\frac{m_x}{\overline{\gamma}_{x,f}}\gamma_{x,f}\right)^k}{k!}\right] \\ &= \frac{1}{\Gamma(m_x)} G_{1,2}^{1,1}\left(\frac{m_x\gamma_{x,f}}{\overline{\gamma}_{x,f}}\middle|\begin{matrix}1\\ m_x,0\end{matrix}\right), \end{aligned} \quad (15)$$

where the second line in (15) represents a the lower incomplete gamma function in terms of the Meijer G function according to [77, 7.11.3].

C. MIXED SIGNAL-TO-NOISE RATIO OF EACH HOP

Both relay node and legitimate receiver Bob apply the maximum ratio combining (MRC) diversity method on the received signals over FSO and RF links. Therefore, the overall electrical SNR in each hop is in fact the sum of the instantaneous electrical SNRs of both links, and it is expressed as

$$\gamma_x = \gamma_{x,o} + \gamma_{x,f}, \quad (16)$$

where $\gamma_{x,o}$ and $\gamma_{x,f}$ denote the instantaneous electrical SNR of the FSO and RF links, respectively. Accordingly, the CDF of the overall SNR in each hop can be obtained by applying a simple change of variable as follows. By letting $\Delta = \gamma_{x,o} + \gamma_{x,f}$, the CDF of Δ can be calculated as

$$\begin{aligned} F_\Delta(\delta) &= \int_{-\infty}^{\infty}\int_{-\infty}^{\delta-\gamma_{x,f}} f_{\gamma_o}(\gamma_{x,o}) f_{\gamma_f}(\gamma_{x,f}) \cdot d\gamma_{x,o} d\gamma_{x,f}, \\ &= \int_0^{\infty} F_{\gamma_o}(\delta-\gamma_{x,f}) f_{\gamma_f}(\gamma_{x,f}) \cdot d\gamma_{x,f}, \end{aligned} \quad (17)$$

by substituting (8) and (13), the integral in (17) is re-written as

$$\begin{aligned} F_\Delta(\delta) &= \frac{1}{\Gamma(\alpha_x)\Gamma(\beta_x)} \frac{m_x^{m_x}}{\Gamma(m_x)\overline{\gamma}_{x,f}^{m_x}} \int_0^{\infty} \gamma_{x,f}^{m_x-1} e^{-\frac{m_x}{\overline{\gamma}_{x,f}}\gamma_{x,f}} \\ &\quad \times G_{1,3}^{2,1}\left(\frac{\alpha_x\beta_x}{\sqrt{\overline{\gamma}_{x,o}}}\sqrt{\delta-\gamma_{x,f}}\middle|\begin{matrix}1\\ \alpha_x,\beta_x,0\end{matrix}\right) \cdot d\gamma_{x,f}, \end{aligned} \quad (18)$$

by applying a change of variable $u = \delta - \gamma_{x,f}$, the integral can be re-written as

$$\begin{aligned} &F_\Delta(\delta) \\ &= \frac{-m^m}{\Gamma(\alpha_x)\Gamma(\beta_x)\Gamma(m)\overline{\gamma}_{x,f}^m} e^{-\frac{m}{\overline{\gamma}_{x,f}}\delta} \\ &\times \int_0^{\infty} (\delta-u)^{m-1} e^{\frac{m}{\overline{\gamma}_{x,f}}u} G_{1,3}^{2,1}\left(\frac{\alpha_x\beta_x}{\sqrt{\overline{\gamma}_{x,o}}}\sqrt{u}\middle|\begin{matrix}1\\ \alpha_x,\beta_x,0\end{matrix}\right) \cdot du, \end{aligned} \quad (19)$$

where the polynomial term can be re-expressed by the use of binomial theorem

$$(\delta-u)^{m-1}=\sum_{\ell=0}^{m-1}\binom{m-1}{\ell}\delta^{m-\ell-1}(-u)^{\ell}, \tag{20}$$

accordingly, the integral can be re-written as

$$\begin{aligned}F_{\Delta}(\delta)=&\frac{-m_x^{m_x}}{\Gamma(\alpha_x)\Gamma(\beta_x)\Gamma(m_x)\overline{\gamma}_{x,f}^{m_x}}e^{-\frac{m_x}{\overline{\gamma}_{x,f}}\delta}\\&\times\sum_{\ell=0}^{m_x-1}\binom{m_x-1}{\ell}(-1)^{\ell}\delta^{m_x-\ell-1}\\&\times\int_0^{\infty}u^{\ell}e^{\frac{m_x}{\overline{\gamma}_{x,f}}u}G_{1,3}^{2,1}\left(\frac{\alpha_x\beta_x}{\sqrt{\overline{\gamma}_{x,o}}}\sqrt{u}\middle|\begin{matrix}1\\ \alpha_x,\ \beta_x,\ 0\end{matrix}\right)\cdot du,\end{aligned} \tag{21}$$

and by using [77, (2.24.3-1)], the resultant integral is solved as

$$\begin{aligned}&F_{\Delta}(\delta)\\&=\frac{-m_x^{m_x}}{\Gamma(\alpha_x)\Gamma(\beta_x)\Gamma(m_x)\overline{\gamma}_{x,f}^{m_x}}e^{-\frac{m_x}{\overline{\gamma}_{x,f}}\delta}\\&\times\sum_{\ell=0}^{m_x-1}\binom{m_x-1}{\ell}(-1)^{\ell}\delta^{m_x-\ell-1}\frac{2^{\alpha_x+\beta_x-1}}{2\pi}\left(-\frac{m_x}{\overline{\gamma}_{x,f}}\right)^{-(\ell+1)}\\&\times G_{3,6}^{4,3}\left(-\frac{\overline{\gamma}_{x,f}}{\overline{\gamma}_{x,o}}\frac{\alpha_x^2\beta_x^2}{16m_x}\middle|\begin{matrix}-\ell,\ \frac{1}{2},\ 1\\ \frac{\alpha_x}{2},\ \frac{\alpha_x+1}{2},\ \frac{\beta_x}{2},\ \frac{\beta_x+1}{2},\ 0,\ \frac{1}{2}\end{matrix}\right),\end{aligned} \tag{22}$$

further, by using a change of variable, (22) can be re-written as

$$F_{\Delta}(\delta)=C_0(x)\sum_{\ell=0}^{m_x-1}C_1(x)\delta^{m_x-\ell-1}e^{-\frac{m_x}{\overline{\gamma}_{x,f}}\delta}, \tag{23}$$

where

$$\begin{aligned}C_0(x)=&-\frac{1}{\Gamma(\alpha_x)\Gamma(\beta_x)}\frac{m_x^{m_x}}{\Gamma(m_x)\overline{\gamma}_{x,f}^{m_x}},\\C_1(x)=&\binom{m_x-1}{\ell}(-1)^{\ell}\frac{2^{\alpha_x+\beta_x-1}}{2\pi}\left(-\frac{m_x}{\overline{\gamma}_{x,f}}\right)^{-(\ell+1)}\\&\times G_{3,6}^{4,3}\left(-\frac{\overline{\gamma}_{x,f}}{\overline{\gamma}_{x,o}}\frac{\alpha_x^2\beta_x^2}{16m_x}\middle|\begin{matrix}-\ell,\ \frac{1}{2},\ 1\\ \frac{\alpha_x}{2},\ \frac{\alpha_x+1}{2},\ \frac{\beta_x}{2},\ \frac{\beta_x+1}{2},\ 0,\ \frac{1}{2}\end{matrix}\right).\end{aligned} \tag{24}$$

Accordingly, the PDF of the overall SNR in each hop is calculated as

$$\begin{aligned}f_{\Delta}(\delta)=&\frac{d}{d\delta}F_{\Delta}(\delta),\\=&\frac{d}{d\delta}\left(C_0(x)\sum_{\ell=0}^{m_x-1}C_1(x)\delta^{m_x-\ell-1}e^{-\frac{m_x}{\overline{\gamma}_{x,f}}\delta}\right),\\=&C_0(x)\sum_{\ell=0}^{m_x-1}C_1(x)(m_x-\ell-2)\delta^{m_x-\ell-3}e^{-\frac{m_x}{\overline{\gamma}_{x,f}}\delta}\\&-\frac{m_x}{\overline{\gamma}_{x,f}}\delta^{m_x-\ell-2}e^{-\frac{m_x}{\overline{\gamma}_{x,f}}\delta}.\end{aligned} \tag{25}$$

III. RELAYING SCHEMES

A. VARIABLE-GAIN RELAYING

In the variable-gain relaying scheme, the relay part exploits the channel state information and the received SNR at destination can be approximated as [78, (5)]

$$\gamma_s^{\mathrm{VG}}=\frac{\gamma_1\gamma_2}{\gamma_1+\gamma_2+1}\approx\min\left(\gamma_1,\gamma_2\right). \tag{26}$$

Such an approximation is accurate in medium and high SNR regimes and has been widely adopted in the literature [79], [80], [81]. Accordingly, the CDF of the SNR at destination is expressed as

$$\begin{aligned}F_{\gamma_s}^{\mathrm{VG}}(\gamma_s)=&\ \mathrm{Prob.}\left(\min\left(\gamma_1,\gamma_2\le\gamma_1\right)\right),\\=&\ F_{\gamma_1}(\gamma_s)+F_{\gamma_2}(\gamma_s)-F_{\gamma_1}(\gamma_s)F_{\gamma_2}(\gamma_s),\end{aligned} \tag{27}$$

then, by substituting (22) into (27), the CDF of the SNR at destination for VG relaying is expressed as

$$\begin{aligned}F_{\gamma_s}^{\mathrm{VG}}(\gamma_s)=&\ C_0(1)\sum_{\ell=0}^{m_1-1}C_1(1)\gamma_s^{m_1-\ell-1}e^{-\frac{m_1}{\overline{\gamma}_{1,f}}\gamma_s}\\&+C_0(2)\sum_{\ell=0}^{m_2-1}C_1(2)\gamma_s^{m_2-\ell-1}e^{-\frac{m_2}{\overline{\gamma}_{2,f}}\gamma_s}\\&-C_0(1)C_0(2)\sum_{\ell=0}^{m_1-1}C_1(1)\sum_{\ell=0}^{m_2-1}C_1(2)\\&\times\gamma_s^{m_1+m_2-2\ell-2}e^{-\left(\frac{m_1}{\overline{\gamma}_{1,f}}+\frac{m_2}{\overline{\gamma}_{2,f}}\right)\gamma_s}.\end{aligned} \tag{28}$$

B. FIXED-GAIN RELAYING

In the fixed-gain relaying scheme, the received SNR at destination is expressed as [78, (6)]

$$\gamma_s^{\mathrm{FG}}=\frac{\gamma_1\gamma_2}{\gamma_2+\mathcal{G}}, \tag{29}$$

where $\mathcal{G}$ denotes the gain of relaying scheme. Accordingly, the CDF of the SNR at destination is expressed as

$$\begin{aligned}F_{\gamma_s}^{\mathrm{FG}}(\gamma_s)=&\ \mathrm{Prob.}\left(\frac{\gamma_1\gamma_2}{\gamma_2+\mathcal{G}}\le\gamma_s\right),\\=&\int_0^{\infty}F_{\gamma_1}\left(\left(1+\frac{\mathcal{G}}{\gamma_2}\right)\gamma_s\right)f_{\gamma_2}(\gamma_2)\cdot d\gamma_2.\end{aligned} \tag{30}$$

by substituting (23) and (25), the integral in (30) is re-written as

$$\begin{aligned}&F_{\gamma_s}^{\mathrm{FG}}(\gamma_s)\\&=\int_0^{\infty}e^{-\frac{m_1}{\overline{\gamma}_{1,f}}\gamma_s}C_0(1)\sum_{\ell_1=0}^{m_1-1}C_1(1)\left(\gamma_s+\frac{\mathcal{G}\gamma_s}{\gamma_2}\right)^{m_1-\ell_1-1}\\&\times e^{-\frac{m_1}{\overline{\gamma}_{1,f}}\frac{\mathcal{G}\gamma_s}{\gamma_2}}C_0(2)\sum_{\ell_2=0}^{m_2-1}C_1(2)(m_2-\ell_2-2)\\&\times\gamma_2^{m_2-\ell_2-3}e^{-\frac{m_2}{\overline{\gamma}_{2,f}}\gamma_2}-\frac{m_2}{\overline{\gamma}_{2,f}}\gamma_2^{m_2-\ell_2-2}e^{-\frac{m_2}{\overline{\gamma}_{2,f}}\gamma_2}\cdot d\gamma_2,\end{aligned} \tag{31}$$

by using binomial theorem, the polynomial term can be re-expressed as

$$\left(\gamma_s+\frac{\mathcal{G}\gamma_s}{\gamma_2}\right)^{m_1-\ell_1-1} = \sum_{k=0}^{m_1-\ell_1-1}\binom{m_1-\ell_1-1}{k}\gamma_s^{m_1-\ell_1-1}\mathcal{G}^k\gamma_2^{-k}, \quad (32)$$

then, the integral in (31) can be re-written as

$$\begin{aligned}F_{\gamma_s}^{\mathrm{FG}}(\gamma_s) &= e^{-\frac{m_1}{\overline{\gamma}_{1,f}}\gamma_s}C_0(1)\sum_{\ell_1=0}^{m_1-1}C_1(1)C_0(2)\sum_{\ell_2=0}^{m_2-1}C_1(2)\\ &\times\sum_{k=0}^{m_1-\ell_1-1}\binom{m_1-\ell_1-1}{k}\mathcal{G}^k\gamma_s^{m_1-\ell_1-1}\\ &\times\Bigg[(m_2-\ell_2-2)\int_0^\infty\gamma_2^{m_2-\ell_2-k-3}e^{-\frac{m_1\mathcal{G}\gamma_s}{\overline{\gamma}_{1,f}\gamma_2}-\frac{m_2}{\overline{\gamma}_{2,f}}\gamma_2}\cdot d\gamma_2\\ &-\frac{m_2}{\overline{\gamma}_{2,f}}\int_0^\infty\gamma_2^{m_2-\ell_2-k-2}e^{-\frac{m_1\mathcal{G}\gamma_s}{\overline{\gamma}_{1,f}\gamma_2}-\frac{m_2}{\overline{\gamma}_{2,f}}\gamma_2}\cdot d\gamma_2\Bigg], \end{aligned}\quad (33)$$

thereafter, by using [82, (2.5.37-2)], the resultant integrals can be solved as in (34), shown at the bottom of the page. Further, by using [83, (11)] and [77, (8.2.2-15)], (34) can be also expressed as in (35), shown at the bottom of the page. Additionally, the parameters B_1, B_2, B_3, $\widehat{B}_2$ and $\widehat{B}_3$, which are used in (34) and (35), are given in Appendix with (105) and (106).

IV. SECRECY PERFORMANCE ANALYSIS

In this section, the physical layer security analysis are presented for the variable-gain and fixed-gain dual-hop relaying schemes using average secrecy capacity, secrecy outage probability, and effective secrecy throughput metrics.

A. AVERAGE SECRECY CAPACITY

Since the wireless communication channels have time-varying nature, secrecy capacity is obtained by averaging the end-to-end instantaneous secrecy capacity that is expressed as [84, (15)]

$$C_S=\int_0^\infty\frac{1}{1+\gamma_b}F_{\gamma_e}(\gamma_b)\big[1-F_{\gamma_b}(\gamma_b)\big]\cdot d\gamma_b, \quad (36)$$

where the term $1/(1+\gamma_b)$ can be expressed in terms of Meijer-G function [77, (8.4.2-5)], and (36) can be re-written as

$$C_S=\int_0^\infty G_{1,1}^{1,1}\left(\gamma_b\middle|\begin{matrix}0\\0\end{matrix}\right)F_{\gamma_e}(\gamma_b)\big[1-F_{\gamma_b}(\gamma_b)\big]\cdot d\gamma_b. \quad (37)$$

1) FSO EAVESDROPPER FOR VARIABLE-GAIN

For the FSO-type eavesdropper, the CDF of SNR $F_{\gamma_e}(\gamma_e)$ is given in (8). Therefore, by substituting (8) and (28) into (37), the ASC is obtained as (54), shown at the bottom of page 9, in terms of $\mathcal{I}_{1,o}^{\mathrm{VG}}$, $\mathcal{I}_{2,o}^{\mathrm{VG}}$, $\mathcal{I}_{3,o}^{\mathrm{VG}}$ and $\mathcal{I}_{4,o}^{\mathrm{VG}}$, which are derived in the following.

The derivation of integral $\mathcal{I}_{1,o}^{\mathrm{VG}}$ is made as follows

$$\mathcal{I}_{1,o}^{\mathrm{VG}}=\int_0^\infty\frac{1}{1+\gamma_b}G_{1,3}^{2,1}\left(\frac{\alpha_e\beta_e}{\sqrt{\overline{\gamma}_{e,o}}}\sqrt{\gamma_b}\middle|\begin{matrix}1\\ \alpha_e,\,\beta_e,\,0\end{matrix}\right)\cdot d\gamma_b, \quad (38)$$

then, the resultant integral is solved by using [77, 2.24.2-4]

$$\mathcal{I}_{1,o}^{\mathrm{VG}}=\frac{2^{\alpha_e+\beta_e-2}}{\pi}G_{3,7}^{5,3}\left(\frac{\alpha_e^2\beta_e^2}{8\overline{\gamma}_{e,o}}\middle|\begin{matrix}0,\,\frac{1}{2},\,1\\ 0,\,\frac{\alpha_e}{2},\,\frac{\alpha_e+1}{2},\,\frac{\beta_e}{2},\,\frac{\beta_e+1}{2},\,0,\,\frac{1}{2}\end{matrix}\right). \quad (39)$$

Since the integrals $\mathcal{I}_{2,o}^{\mathrm{VG}}$, $\mathcal{I}_{3,o}^{\mathrm{VG}}$ and $\mathcal{I}_{4,o}^{\mathrm{VG}}$ follow the same form with different parameters, their derivations can be made as

$$\mathcal{I}_{\upsilon,o}^{\mathrm{VG}}=\int_0^\infty\gamma_b^{a_1}e^{-a_2\gamma_b}G_{1,1}^{1,1}\left(\gamma_b\middle|\begin{matrix}0\\0\end{matrix}\right)$$

$$\begin{aligned}F_{\gamma_s}^{\mathrm{FG}}(\gamma_s) &= C_0(1)\sum_{\ell_1=0}^{m_1-1}C_1(1)C_0(2)\sum_{\ell_2=0}^{m_2-1}C_1(2)\sum_{k=0}^{m_1-\ell_1-1}B_1\\ &\times\Bigg[B_2\gamma_s^{\frac{2m_1+m_2-2\ell_1-\ell_2-k-5}{2}}e^{-\frac{m_1}{\overline{\gamma}_{1,f}}\gamma_s}G_{0,2}^{2,0}\left(\frac{\mathcal{G}m_1m_2}{\overline{\gamma}_{1,f}\overline{\gamma}_{2,f}}\gamma_s\middle|\begin{matrix}-,\,-\\ \frac{m_2-\ell_2-k-2}{2},\,\frac{m_2-\ell_2-k-2}{2}\end{matrix}\right)\\ &-B_3\gamma_s^{\frac{2m_1+m_2-2\ell_1-\ell_2-k-3}{2}}e^{-\frac{m_1}{\overline{\gamma}_{1,f}}\gamma_s}G_{0,2}^{2,0}\left(\frac{\mathcal{G}m_1m_2}{\overline{\gamma}_{1,f}\overline{\gamma}_{2,f}}\gamma_s\middle|\begin{matrix}-,\,-\\ \frac{m_2-\ell_2-k-1}{2},\,\frac{m_2-\ell_2-k-1}{2}\end{matrix}\right)\Bigg]. \end{aligned}\quad (34)$$

$$\begin{aligned}F_{\gamma_s}^{\mathrm{FG}}(\gamma_s) &= C_0(1)\sum_{\ell_1=0}^{m_1-1}C_1(1)C_0(2)\sum_{\ell_2=0}^{m_2-1}C_1(2)\sum_{k=0}^{m_1-\ell_1-1}B_1\\ &\times\Bigg[\widehat{B}_2G_{0,1}^{1,0}\left(\frac{m_1}{\overline{\gamma}_{1,f}}\gamma_s\middle|\begin{matrix}-\\ \frac{2m_1+m_2-2\ell_1-\ell_2-k-5}{2}\end{matrix}\right)G_{0,2}^{2,0}\left(\frac{\mathcal{G}m_1m_2}{\overline{\gamma}_{1,f}\overline{\gamma}_{2,f}}\gamma_s\middle|\begin{matrix}-,\,-\\ \frac{m_2-\ell_2-k-2}{2},\,\frac{m_2-\ell_2-k-2}{2}\end{matrix}\right)\\ &-\widehat{B}_3G_{0,1}^{1,0}\left(\frac{m_1}{\overline{\gamma}_{1,f}}\gamma_s\middle|\begin{matrix}-\\ \frac{2m_1+m_2-2\ell_1-\ell_2-k-3}{2}\end{matrix}\right)G_{0,2}^{2,0}\left(\frac{\mathcal{G}m_1m_2}{\overline{\gamma}_{1,f}\overline{\gamma}_{2,f}}\gamma_s\middle|\begin{matrix}-,\,-\\ \frac{m_2-\ell_2-k-1}{2},\,\frac{m_2-\ell_2-k-1}{2}\end{matrix}\right)\Bigg]. \end{aligned}\quad (35)$$

$$\times G_{1,3}^{2,1}\left(\frac{\alpha_e\beta_e}{\sqrt{\overline{\gamma}_{e,o}}}\sqrt{\gamma_b}\middle|\begin{matrix}1\\ \alpha_e,\,\beta_e,\,0\end{matrix}\right)\cdot d\gamma_b, \quad (40)$$

where the power and exponential terms can be expressed in terms of Meijer-G function by using [83, (11)] and [77, 8.2.2-15]

$$e^{-a_2\gamma_b} = G_{0,1}^{1,0}\left(a_2\gamma_b\middle|\begin{matrix}-\\ 0\end{matrix}\right), \quad (41)$$

$$\gamma_b^{a_1} G_{1,1}^{1,1}\left(\gamma_b\middle|\begin{matrix}0\\ 0\end{matrix}\right) = G_{1,1}^{1,1}\left(\gamma_b\middle|\begin{matrix}a_1\\ a_1\end{matrix}\right), \quad (42)$$

therefore, the integral in (40) is written as

$$\mathcal{I}_{\upsilon,o}^{\mathrm{VG}} = \int_0^\infty G_{1,1}^{1,1}\left(\gamma_b\middle|\begin{matrix}a_1\\ a_1\end{matrix}\right) G_{0,1}^{1,0}\left(a_2\gamma_b\middle|\begin{matrix}-\\ 0\end{matrix}\right) \times G_{1,3}^{2,1}\left(\frac{\alpha_e\beta_e}{\sqrt{\overline{\gamma}_{e,o}}}\sqrt{\gamma_b}\middle|\begin{matrix}1\\ \alpha_e,\,\beta_e,\,0\end{matrix}\right)\cdot d\gamma_b, \quad (43)$$

and the resultant integral can be solved in terms of extended generalized bivariate Meijer-G (EGBMG) function by using [85, (20)]

$$\mathcal{I}_{\upsilon,o}^{\mathrm{VG}} = G_{1,1:0,1:1,3}^{1,1:1,0:2,1}\left(\begin{matrix}a_1+1\\ a_1+1\end{matrix}\middle|\begin{matrix}-\\ 0\end{matrix}\middle|\begin{matrix}1\\ \alpha_e,\,\beta_e,\,0\end{matrix}\middle|a_2,\,\frac{\alpha_e\beta_e}{\sqrt{\overline{\gamma}_{e,o}}}\right), \quad (44)$$

where $\upsilon \in \{2, 3, 4\}$, and the parameters a_1 and a_2 are given in Appendix with (96).

2) RF EAVESDROPPER FOR VARIABLE-GAIN

For the RF-type eavesdropper, the CDF of SNR $F_{\gamma_e}(\gamma_e)$ is given in (15). Therefore, by substituting (15) and (28) into (37), the ASC is obtained as (55), shown at the bottom of the next page, in terms of $\mathcal{I}_{1,f}^{\mathrm{VG}}$, $\mathcal{I}_{2,f}^{\mathrm{VG}}$, $\mathcal{I}_{3,f}^{\mathrm{VG}}$ and $\mathcal{I}_{4,f}^{\mathrm{VG}}$, which are derived in the following.

The derivation of integral $\mathcal{I}_{1,f}^{\mathrm{VG}}$ is made as follows

$$\mathcal{I}_{1,f}^{\mathrm{VG}} = \int_0^\infty G_{1,1}^{1,1}\left(\gamma_b\middle|\begin{matrix}0\\ 0\end{matrix}\right) G_{1,2}^{1,1}\left(\frac{\gamma_b}{\overline{\gamma}_{e,f}}\middle|\begin{matrix}1\\ m_e,\,0\end{matrix}\right)\cdot d\gamma_b, \quad (45)$$

then, the resultant integral is solved by using [76, 7.811-1]

$$\mathcal{I}_{1,f}^{\mathrm{VG}} = G_{2,3}^{2,2}\left(\frac{1}{\overline{\gamma}_{e,f}}\middle|\begin{matrix}0,\,1\\ 0,\,m_e,\,0\end{matrix}\right). \quad (46)$$

Since the integrals $\mathcal{I}_{2,f}^{\mathrm{VG}}$, $\mathcal{I}_{3,f}^{\mathrm{VG}}$ and $\mathcal{I}_{4,f}^{\mathrm{VG}}$ have the same form with different parameters, their derivations can be made as

$$\mathcal{I}_{\upsilon,f}^{\mathrm{VG}} = \int_0^\infty \gamma_b^{a_1} e^{-a_2\gamma_b} G_{1,1}^{1,1}\left(\gamma_b\middle|\begin{matrix}0\\ 0\end{matrix}\right) G_{1,2}^{1,1}\left(\frac{\gamma_{b,f}}{\overline{\gamma}_{e,f}}\middle|\begin{matrix}1\\ m_e,\,0\end{matrix}\right)\cdot d\gamma_b, \quad (47)$$

where the power and exponential terms can be expressed in terms of Meijer-G function by using [77, 8.2.2-15]

$$\gamma_b^{a_1} G_{1,1}^{1,1}\left(\gamma_b\middle|\begin{matrix}0\\ 0\end{matrix}\right) = G_{1,1}^{1,1}\left(\gamma_b\middle|\begin{matrix}a_1\\ a_1\end{matrix}\right), \quad (48)$$

$$e^{-a_2\gamma_b} = G_{0,1}^{1,0}\left(a_2\gamma_b\middle|\begin{matrix}-\\ 0\end{matrix}\right), \quad (49)$$

therefore, the integral in (47) is written as

$$\mathcal{I}_{\upsilon,f}^{\mathrm{VG}} = \int_0^\infty G_{0,1}^{1,0}\left(a_2\gamma_b\middle|\begin{matrix}-\\ 0\end{matrix}\right) G_{1,1}^{1,1}\left(\gamma_b\middle|\begin{matrix}a_1\\ a_1\end{matrix}\right) \times G_{1,2}^{1,1}\left(\frac{\gamma_b}{\overline{\gamma}_{e,f}}\middle|\begin{matrix}1\\ m_e,\,0\end{matrix}\right)\cdot d\gamma_b, \quad (50)$$

and the resultant integral can be solved in terms of EGBMG function by using [85, (20)]

$$\mathcal{I}_{\upsilon,f}^{\mathrm{VG}} = G_{1,1:0,1:1,2}^{1,1:1,0:1,1}\left(\begin{matrix}a_1+1\\ a_1+1\end{matrix}\middle|\begin{matrix}-\\ 0\end{matrix}\middle|\begin{matrix}1\\ m_e,\,0\end{matrix}\middle|a_2,\,\frac{1}{\overline{\gamma}_{e,f}}\right), \quad (51)$$

where $\upsilon \in \{2, 3, 4\}$, and the parameters a_1 and a_2 are given in Appendix with (96).

3) HYBRID EAVESDROPPER FOR VARIABLE-GAIN

For the hybrid-type eavesdropper, the CDF of SNR $F_{\gamma_e}(\gamma_e)$ is given in (23). Therefore, by substituting (23) and (28) into (37), the ASC is obtained as (56), shown at the bottom of the next page, in terms of $\mathcal{I}_{1,h}^{\mathrm{VG}}$, $\mathcal{I}_{2,h}^{\mathrm{VG}}$, $\mathcal{I}_{3,h}^{\mathrm{VG}}$ and $\mathcal{I}_{4,h}^{\mathrm{VG}}$, which are derived in the following.

Since the integrals $\mathcal{I}_{1,h}^{\mathrm{VG}}$, $\mathcal{I}_{2,h}^{\mathrm{VG}}$, $\mathcal{I}_{3,h}^{\mathrm{VG}}$ and $\mathcal{I}_{4,h}^{\mathrm{VG}}$ are in the same form with different parameters, their derivations can be made as

$$\mathcal{I}_{\upsilon,h}^{\mathrm{VG}} = \int_0^\infty \gamma_b^{a_1} e^{-a_2} G_{1,1}^{1,1}\left(\gamma_b\middle|\begin{matrix}0\\ 0\end{matrix}\right)\cdot d\gamma_b, \quad (52)$$

then, the resultant integral is solved by using [76, 7.813-1]

$$\mathcal{I}_{\upsilon,h}^{\mathrm{VG}} = a_2^{-a_1-1} G_{2,1}^{1,2}\left(\frac{1}{a_2}\middle|\begin{matrix}-a_1,\,0\\ 0\end{matrix}\right), \quad (53)$$

where $\upsilon \in \{1, 2, 3, 4\}$, and the parameters a_1 and a_2 are given in Appendix with (97).

4) FSO EAVESDROPPER FOR FIXED-GAIN

For the FSO-type eavesdropper considering FG relay scheme, the CDF of SNR $F_{\gamma_e}(\gamma_e)$ is given in (8). Therefore, by substituting (8) and (34) into (37), the ASC is obtained as (66), shown at the bottom of page 10, in terms of $\mathcal{I}_{1,o}^{\mathrm{FG}}$, $\mathcal{I}_{2,o}^{\mathrm{FG}}$ and $\mathcal{I}_{3,o}^{\mathrm{FG}}$, which are derived in the following.

The derivation of integral $\mathcal{I}_{1,o}^{\mathrm{FG}}$ is the same as $\mathcal{I}_{1,o}^{\mathrm{VG}}$ and is derived in (39).

Since the integrals $\mathcal{I}_{2,o}^{\mathrm{FG}}$ and $\mathcal{I}_{3,o}^{\mathrm{FG}}$ are in the same form with different parameters, their derivations can be made as follows

$$\mathcal{I}_{\upsilon,o}^{\mathrm{FG}} = \int_0^\infty \gamma_s^{a_1} e^{-b_1\gamma_s} G_{1,1}^{1,1}\left(\gamma_s\middle|\begin{matrix}0\\ 0\end{matrix}\right) G_{0,2}^{2,0}\left(b_2\gamma_s\middle|\begin{matrix}-,\,-\\ a_2,\,a_2\end{matrix}\right) \times G_{1,3}^{2,1}\left(\alpha_e\beta_e\sqrt{\gamma_s}\middle|\begin{matrix}1\\ \alpha_e,\,\beta_e,\,0\end{matrix}\right)\cdot d\gamma_s, \quad (57)$$

then, by using the series expansion of exponential function and the equality in [77, 8.2.2-15], the integral is re-expressed as

$$\mathcal{I}_{\upsilon,o}^{\mathrm{FG}} = \sum_{n=0}^{\infty}\frac{(-b_1)^n}{n!}\int_0^\infty G_{0,2}^{2,0}\left(b_2\gamma_s\middle|\begin{matrix}-,\,-\\ a_2,\,a_2\end{matrix}\right) G_{1,1}^{1,1}\left(\gamma_s\middle|\begin{matrix}n+a_1\\ n+a_1\end{matrix}\right)$$

$$\times G_{1,3}^{2,1}\left(\alpha_x\beta_x\sqrt{\gamma_s}\middle|\begin{matrix}1\\ \alpha_x,\,\beta_x,\,0\end{matrix}\right)\cdot d\gamma_s, \quad (58)$$

and the resultant integral can be solved in terms of EGBMG function by using [85, (20)]

$$\mathcal{I}_{\upsilon,o}^{\mathrm{FG}} = \sum_{n=0}^{\infty}\frac{(-b_1)^n}{n!} \times G_{1,1:0,2:1,3}^{1,1:2,0:2,1}\left(\begin{matrix}n+a_1+1\\ n+a_1+1\end{matrix}\middle|\begin{matrix}-,-\\ a_2,\,a_2\end{matrix}\middle|\begin{matrix}1\\ \alpha_e,\,\beta_e,\,0\end{matrix}\middle|b_2,\,\frac{\alpha_e\beta_e}{\sqrt{\overline{\gamma}_{e,o}}}\right), \quad (59)$$

where $\upsilon \in \{2, 3\}$, and the parameters a_1, a_2, b_1, b_2 are given in Appendix with (98).

5) RF EAVESDROPPER FOR FIXED-GAIN

For the RF-type eavesdropper considering FG relay scheme, the CDF of SNR $F_{\gamma_e}(\gamma_e)$ is given in (15). Therefore, by substituting (15) and (34) into (37), the ASC is obtained as (67), shown at the bottom of the next page, in terms of $\mathcal{I}_{1,f}^{\mathrm{FG}}$, $\mathcal{I}_{2,f}^{\mathrm{FG}}$ and $\mathcal{I}_{3,f}^{\mathrm{FG}}$, which are derived in the following.

The derivation of integral $\mathcal{I}_{1,f}^{\mathrm{FG}}$ is the same as $\mathcal{I}_{1,f}^{\mathrm{VG}}$ and is derived in (46).

Since the integrals $\mathcal{I}_{2,f}^{\mathrm{FG}}$ and $\mathcal{I}_{3,f}^{\mathrm{FG}}$ are in the same form with different parameters, their derivations can be made as follows

$$\mathcal{I}_{\upsilon,f}^{\mathrm{FG}} = \int_0^{\infty}\gamma_s^{a_1}e^{-b_1\gamma_s}G_{1,1}^{1,1}\left(\gamma_s\middle|\begin{matrix}0\\ 0\end{matrix}\right)G_{0,2}^{2,0}\left(b_2\gamma_s\middle|\begin{matrix}-,-\\ a_2,\,a_2\end{matrix}\right) \times G_{1,2}^{1,1}\left(\frac{\gamma_s}{\overline{\gamma}_{e,f}}\middle|\begin{matrix}1\\ m_x,\,0\end{matrix}\right)\cdot d\gamma_s \quad (60)$$

then, by using the series expansion of exponential function and the equality in [77, 8.2.2-15], the integral is re-expressed as

$$\mathcal{I}_{\upsilon,f}^{\mathrm{FG}} = \sum_{n=0}^{\infty}\frac{(-b_1)^n}{n!}\int_0^{\infty}G_{0,2}^{2,0}\left(b_2\gamma_s\middle|\begin{matrix}-,-\\ a_2,\,a_2\end{matrix}\right)G_{1,1}^{1,1}\left(\gamma_s\middle|\begin{matrix}n+a_1\\ n+a_1\end{matrix}\right) \times G_{1,2}^{1,1}\left(\frac{\gamma_s}{\overline{\gamma}_{e,f}}\middle|\begin{matrix}1\\ m_e,\,0\end{matrix}\right)\cdot d\gamma_s \quad (61)$$

and the resultant integral can be solved in terms of EGBMG function by using [85, (20)]

$$\mathcal{I}_{\upsilon,f}^{\mathrm{FG}} = \sum_{n=0}^{\infty}\frac{(-b_1)^n}{n!} \times G_{1,1:0,2:1,3}^{1,1:2,0:2,1}\left(\begin{matrix}n+a_1+1\\ n+a_1+1\end{matrix}\middle|\begin{matrix}-,-\\ a_2,\,a_2\end{matrix}\middle|\begin{matrix}1\\ \alpha_e,\,\beta_e,\,0\end{matrix}\middle|b_2,\,\frac{1}{\overline{\gamma}_{e,f}}\right), \quad (62)$$

where $\upsilon \in \{2, 3\}$, and the parameters a_1, a_2, b_1, b_2 are given in Appendix with (98).

6) HYBRID EAVESDROPPER FOR FIXED-GAIN

For the hybrid-type eavesdropper, the CDF of SNR $F_{\gamma_e}(\gamma_e)$ is given in (23). Therefore, by substituting (23) and (34) into (37), the ASC is obtained as (68), shown at the bottom of the next page, in terms of $\mathcal{I}_{1,h}^{\mathrm{FG}}$, $\mathcal{I}_{2,h}^{\mathrm{FG}}$ and $\mathcal{I}_{3,h}^{\mathrm{FG}}$, which are derived in the following.

The derivation of integral $\mathcal{I}_{1,h}^{\mathrm{FG}}$ is the same as $\mathcal{I}_{1,h}^{\mathrm{VG}}$ and is derived in (53).

Since the integrals $\mathcal{I}_{2,h}^{\mathrm{FG}}$ and $\mathcal{I}_{3,h}^{\mathrm{FG}}$ are in the same form with different parameters, their derivations can be made as

$$\mathcal{I}_{\upsilon,o}^{\mathrm{FG}} = \int_0^{\infty}\gamma_b^{a_1}e^{-b_1\gamma_b}G_{1,1}^{1,1}\left(\gamma_b\middle|\begin{matrix}0\\ 0\end{matrix}\right)G_{0,2}^{2,0}\left(b_2\gamma_b\middle|\begin{matrix}-,-\\ a_2,\,a_2\end{matrix}\right)\cdot d\gamma_b, \quad (63)$$

$$C_S^{\mathrm{FSO,VG}} = \frac{1}{\Gamma(\alpha_e)\Gamma(\beta_e)}\Bigg[\mathcal{I}_{1,o}^{\mathrm{VG}} - C_0(1)\sum_{\ell=0}^{m_1-1}C_1(1)\mathcal{I}_{2,o}^{\mathrm{VG}} - C_0(2)\sum_{\ell=0}^{m_2-1}C_1(2)\mathcal{I}_{3,o}^{\mathrm{VG}} + C_0(1)C_0(2) \times \sum_{\ell=0}^{m_1-1}C_1(1)\sum_{\ell=0}^{m_2-1}C_1(2)\mathcal{I}_{4,o}^{\mathrm{VG}}\Bigg], \quad (54)$$

$$C_S^{\mathrm{RF,VG}} = \frac{1}{\Gamma(m_e)}\Bigg[\mathcal{I}_{1,f}^{\mathrm{VG}} - C_0(1)\sum_{\ell=0}^{m_1-1}C_1(1)\mathcal{I}_{2,f}^{\mathrm{VG}} - C_0(2)\sum_{\ell=0}^{m_2-1}C_1(2)\mathcal{I}_{3,f}^{\mathrm{VG}} + C_0(1)C_0(2) \times \sum_{\ell=0}^{m_1-1}C_1(1)\sum_{\ell=0}^{m_2-1}C_1(2)\mathcal{I}_{4,f}^{\mathrm{VG}}\Bigg], \quad (55)$$

$$C_S^{\mathrm{HYB,VG}} = C_0(e)\sum_{\ell_e=0}^{m_e-1}C_1(e)\Bigg[\mathcal{I}_{1,h}^{\mathrm{VG}} - C_0(1)\sum_{\ell=0}^{m_1-1}C_1(1)\mathcal{I}_{2,h}^{\mathrm{VG}} - C_0(2) \times \sum_{\ell=0}^{m_2-1}C_1(2)\mathcal{I}_{3,h}^{\mathrm{VG}} + C_0(1)C_0(2)\sum_{\ell=0}^{m_1-1}C_1(1)\sum_{\ell=0}^{m_2-1}C_1(2)\mathcal{I}_{4,h}^{\mathrm{VG}}\Bigg]. \quad (56)$$

by using [83, (11)] and [77, (8.2.2-15)], the integral can be re-expressed as

$$\mathcal{I}_{\upsilon,o}^{\mathrm{FG}} = b_1^{-a_1} \int_0^{\infty} G_{0,1}^{1,0}\left(b_1\gamma_b \middle| \begin{matrix} - \\ a_1 \end{matrix}\right) G_{1,1}^{1,1}\left(\gamma_b \middle| \begin{matrix} 0 \\ 0 \end{matrix}\right) \times G_{0,2}^{2,0}\left(b_2\gamma_b \middle| \begin{matrix} -, - \\ a_2, a_2 \end{matrix}\right) \cdot d\gamma_b, \quad (64)$$

and the resultant integral can be solved in terms of EGBMG function by using [85, (20)]

$$\mathcal{I}_{\upsilon,f}^{\mathrm{FG}} = b_1^{-a_1} G_{1,1:0,1:0,2}^{1,1:1,0:2,0}\left(\begin{matrix} 1 \\ 1 \end{matrix} \middle| \begin{matrix} - \\ a_1 \end{matrix} \middle| \begin{matrix} -, - \\ a_2, a_2 \end{matrix} \middle| b_1, b_2\right), \quad (65)$$

where $\upsilon \in \{2, 3\}$, and the parameters a_1, a_2, b_1, b_2 are given in Appendix with (99).

B. SECRECY OUTAGE PROBABILITY

The metric secrecy outage probability (SOP) is widely used to characterize the secure communication between legitimate pairs, which is described the probability that the instantaneous secrecy capacity falls below a target secrecy rate $\mathcal{R}$, defined as [44, (10)]

$$\begin{aligned} P_{SO} &= \mathrm{Prob.}\big(C_S(\gamma_b, \gamma_e) \le \mathcal{R}\big), \\ &= \mathrm{Prob.}\big(\gamma_b \le 2^{\mathcal{R}}(\gamma_e + 1) - 1\big), \\ &= \int_0^{\infty} F_{\gamma_b}\big(2^{\mathcal{R}}(\gamma_e + 1) - 1\big) f_{\gamma_e}(\gamma_e) \cdot d\gamma_e, \end{aligned} \quad (69)$$

where $\mathcal{R} > 0$. It is worthy to note that in some cases, an exact closed-form expression of SOP is not available due to the shifting operation in some special functions. However, instead, a lower bound of SOP can be derived as follows [44, (11)]

$$\begin{aligned} P_{SO} &= \mathrm{Prob.}\big(\gamma_b \le 2^{\mathcal{R}}(\gamma_e + 1) - 1\big), \\ \ge P_{SO_L} &= \mathrm{Prob.}\big(\gamma_b \le 2^{\mathcal{R}}\gamma_e\big), \\ &= \int_0^{\infty} F_{\gamma_b}\big(2^{\mathcal{R}}\gamma_e\big) f_{\gamma_e}(\gamma_e) \cdot d\gamma_e. \end{aligned} \quad (70)$$

1) FSO EAVESDROPPER FOR VARIABLE-GAIN

For the FSO-type eavesdropper, the PDF of SNR $f_{\gamma_e}(\gamma_e)$ is given in (7). Therefore, by substituting (7) and (28) into (69), the SOP is obtained as (77), shown at the bottom of the next page, in terms of $\mathcal{T}_{1,o}^{\mathrm{VG}}$, $\mathcal{T}_{2,o}^{\mathrm{VG}}$ and $\mathcal{T}_{3,o}^{\mathrm{VG}}$.

Since the integrals $\mathcal{T}_{1,o}^{\mathrm{VG}}$, $\mathcal{T}_{2,o}^{\mathrm{VG}}$ and $\mathcal{T}_{3,o}^{\mathrm{VG}}$ are in the same form with different parameters, their derivations can be made as

$$\mathcal{T}_{\upsilon,o}^{\mathrm{VG}} = \int_0^{\infty} \gamma_e^{a_1 - 1} e^{-a_2\gamma_e} \times G_{0,2}^{2,0}\left(\frac{\alpha_e\beta_e}{\sqrt{\overline{\gamma}_{e,o}}}\sqrt{\gamma_e} \middle| \begin{matrix} -, - \\ \frac{\alpha_e - \beta_e}{2}, \frac{\alpha_e - \beta_e}{2} \end{matrix}\right) \cdot d\gamma_e, \quad (71)$$

then, the resultant integral is solved by using [77, 2.24.1-1]

$$\mathcal{T}_{\upsilon,o}^{\mathrm{VG}} = \frac{2^{\alpha_e - \beta_e} a_2^{-a_1}}{2\pi} \times G_{1,4}^{4,1}\left(\frac{\alpha_e^2\beta_e^2}{8a_2\overline{\gamma}_{e,o}} \middle| \begin{matrix} 1 - a_1 \\ \frac{\alpha_e - \beta_e}{4}, \frac{\alpha_e - \beta_e + 1}{4}, \frac{\alpha_e - \beta_e}{4}, \frac{\alpha_e - \beta_e + 1}{4} \end{matrix}\right), \quad (72)$$

where $\upsilon \in \{1, 2, 3\}$, and the parameters a_1 and a_2 are given in Appendix with (100).

2) RF EAVESDROPPER FOR VARIABLE-GAIN

For the RF-type eavesdropper, the PDF of SNR $f_{\gamma_e}(\gamma_e)$ is given in (13). Therefore, by substituting (13) and (28) into (69), the SOP is obtained as (78), shown at the bottom of the next page, in terms of $\mathcal{T}_{1,f}^{\mathrm{VG}}$, $\mathcal{T}_{2,f}^{\mathrm{VG}}$ and $\mathcal{T}_{3,f}^{\mathrm{VG}}$.

Since the integrals $\mathcal{T}_{1,o}^{\mathrm{VG}}$, $\mathcal{T}_{2,o}^{\mathrm{VG}}$ and $\mathcal{T}_{3,o}^{\mathrm{VG}}$ are in the same form with different parameters, their derivations can be made as

$$\mathcal{T}_{\upsilon,f}^{\mathrm{VG}} = \int_0^{\infty} \gamma_e^{a_1} e^{-a_2\gamma_e} \cdot d\gamma_e, \quad (73)$$

then, the resultant integral is solved by using [76, 3.351-3]

$$\mathcal{T}_{\upsilon,f}^{\mathrm{VG}} = a_1! a_2^{-a_1 - 1}, \quad (74)$$

where $\upsilon \in \{1, 2, 3\}$, and the parameters a_1 and a_2 are given in Appendix with (101).

3) HYBRID EAVESDROPPER FOR VARIABLE-GAIN

For the hybrid-type eavesdropper, the PDF of SNR $f_{\gamma_e}(\gamma_e)$ is given in (25). Therefore, by substituting (25) and (28) into (69), the SOP is obtained as (79), shown at the bottom of the next page, in terms of $\mathcal{T}_{1,o}^{\mathrm{VG}}$, $\mathcal{T}_{2,o}^{\mathrm{VG}}$, $\mathcal{T}_{3,o}^{\mathrm{VG}}$, $\mathcal{T}_{4,o}^{\mathrm{VG}}$, $\mathcal{T}_{5,o}^{\mathrm{VG}}$ and $\mathcal{T}_{6,o}^{\mathrm{VG}}$.

$$C_S^{\mathrm{FSO,FG}} = \frac{1}{\Gamma(\alpha_e)\Gamma(\beta_e)}\left(\mathcal{I}_{1,o}^{\mathrm{FG}} - C_0(1)\sum_{\ell_1=0}^{m_1-1} C_1(1)C_0(2)\sum_{\ell_2=0}^{m_2-1} C_1(2)\sum_{k=0}^{m_1-\ell_1-1} B_1\left[B_2\mathcal{I}_{2,o}^{\mathrm{FG}} - B_3\mathcal{I}_{3,o}^{\mathrm{FG}}\right]\right) \quad (66)$$

$$C_S^{\mathrm{RF,FG}} = \frac{1}{\Gamma(m_e)}\left(\mathcal{I}_{1,f}^{\mathrm{FG}} - C_0(1)\sum_{\ell_1=0}^{m_1-1} C_1(1)C_0(2)\sum_{\ell_2=0}^{m_2-1} C_1(2)\sum_{k=0}^{m_1-\ell_1-1} B_1\left[B_2\mathcal{I}_{2,f}^{\mathrm{FG}} - B_3\mathcal{I}_{3,f}^{\mathrm{FG}}\right]\right) \quad (67)$$

$$C_S^{\mathrm{HYB,FG}} = C_0(e)\sum_{\ell_e=0}^{m_e-1} C_1(e)\left(\mathcal{I}_{1,h}^{\mathrm{FG}} - C_0(1)\sum_{\ell_1=0}^{m_1-1} C_1(1)C_0(2)\sum_{\ell_2=0}^{m_2-1} C_1(2)\sum_{k=0}^{m_1-\ell_1-1} B_1\left[B_2\mathcal{I}_{2,h}^{\mathrm{FG}} - B_3\mathcal{I}_{3,h}^{\mathrm{FG}}\right]\right) \quad (68)$$

Similar to the RF eavesdropper case for VG case, $\mathcal{T}_{1,o}^{\mathrm{VG}}$, $\mathcal{T}_{2,o}^{\mathrm{VG}}$, $\mathcal{T}_{3,o}^{\mathrm{VG}}$, $\mathcal{T}_{4,o}^{\mathrm{VG}}$, $\mathcal{T}_{5,o}^{\mathrm{VG}}$ and $\mathcal{T}_{6,o}^{\mathrm{VG}}$ are in the same form with different parameters, their derivations can be made as

$$\mathcal{T}_{\upsilon,f}^{\mathrm{VG}} = \int_0^{\infty} \gamma_e^{a_1} e^{-a_2\gamma_e} \cdot d\gamma_e, \tag{75}$$

then, the resultant integral is solved by using [76, 3.351-3]

$$\mathcal{T}_{\upsilon,f}^{\mathrm{VG}} = a_1! a_2^{-a_1-1}, \tag{76}$$

where $\upsilon \in \{1, 2, 3, 4, 5, 6\}$, and the parameters a_1 and a_2 are given in Appendix with (102).

4) FSO EAVESDROPPER FOR FIXED-GAIN

For the FSO-type eavesdropper considering FG relay scheme, the PDF of SNR $f_{\gamma_e}(\gamma_e)$ is given in (7). Accordingly, by substituting (7) and (35) into (70), the lower bound of SOP is obtained as (86), shown at the bottom of the next page, in terms of $\mathcal{T}_{1,o}^{\mathrm{FG}}$, and $\mathcal{T}_{2,o}^{\mathrm{FG}}$.

Since the integrals $\mathcal{T}_{1,o}^{\mathrm{FG}}$ and $\mathcal{T}_{2,o}^{\mathrm{FG}}$ are in the same form with different parameters, their derivations can be made as

$$\mathcal{T}_{\upsilon,o}^{\mathrm{FG}} = \int_0^{\infty} G_{0,1}^{1,0}\left(\frac{m_1 2^{\mathcal{R}}}{\overline{\gamma}_{1,f}}\gamma_e \middle| \begin{matrix} - \\ a_1 \end{matrix}\right) G_{0,2}^{2,0}\left(\frac{\mathcal{G} m_1 m_2 2^{\mathcal{R}}}{\overline{\gamma}_{1,f}\overline{\gamma}_{2,f}}\gamma_e \middle| \begin{matrix} -, - \\ a_2, a_2 \end{matrix}\right) \times G_{0,2}^{2,0}\left(\frac{\alpha_e\beta_e}{\sqrt{\overline{\gamma}_{e,o}}}\sqrt{\gamma_e} \middle| \begin{matrix} -, - \\ \frac{\alpha_e-\beta_e}{2}, \frac{\alpha_e-\beta_e}{2} \end{matrix}\right) \cdot d\gamma_e, \tag{80}$$

and the resultant integral can be solved in terms of EGBMG function by using [85, (20)]

$$\mathcal{T}_{\upsilon,o}^{\mathrm{FG}} = \frac{\overline{\gamma}_{1,f}}{m_1 2^{\mathcal{R}}} G_{0,1:0,2:0,2}^{1,0:2,0:2,0} \times \left(\begin{matrix} a_1+1 \\ - \end{matrix} \middle| \begin{matrix} -, - \\ a_2, a_2 \end{matrix} \middle| \begin{matrix} -, - \\ \frac{\alpha_e-\beta_e}{2}, \frac{\alpha_e-\beta_e}{2} \end{matrix} \middle| \begin{matrix} \frac{\mathcal{G} m_2}{\overline{\gamma}_{2,f}}, \frac{\alpha_e\beta_e\overline{\gamma}_{1,f}}{m_1 2^{\mathcal{R}}\sqrt{\overline{\gamma}_{e,o}}} \end{matrix}\right), \tag{81}$$

where $\upsilon \in \{1, 2\}$, and the parameters a_1 and a_2 are given in Appendix with (103).

5) RF EAVESDROPPER FOR FIXED-GAIN

For the RF-type eavesdropper considering FG relay scheme, the PDF of SNR $f_{\gamma_e}(\gamma_e)$ is given in (13). Therefore, by substituting (13) and (35) into (70), the lower bound of SOP is obtained as (87), shown at the bottom of the next page, in terms of $\mathcal{T}_{1,f}^{\mathrm{FG}}$, and $\mathcal{T}_{2,f}^{\mathrm{FG}}$.

Since the integrals $\mathcal{T}_{1,f}^{\mathrm{FG}}$ and $\mathcal{T}_{2,f}^{\mathrm{FG}}$ are in the same form with different parameters, their derivations can be made as

$$\mathcal{T}_{\upsilon,f}^{\mathrm{FG}} = \int_0^{\infty} G_{0,1}^{1,0}\left(\frac{m_1 2^{\mathcal{R}}}{\overline{\gamma}_{1,f}}\gamma_e \middle| \begin{matrix} - \\ a_1 \end{matrix}\right) \times G_{0,2}^{2,0}\left(\frac{\mathcal{G} m_1 m_2 2^{\mathcal{R}}}{\overline{\gamma}_{1,f}\overline{\gamma}_{2,f}}\gamma_e \middle| \begin{matrix} -, - \\ a_2, a_2 \end{matrix}\right) \times G_{0,1}^{1,0}\left(\frac{m_e}{\overline{\gamma}_{e,f}}\gamma_e \middle| \begin{matrix} - \\ m_e - 1 \end{matrix}\right) \cdot d\gamma_e, \tag{82}$$

and the resultant integral can be solved in terms of EGBMG function by using [85, (20)]

$$\mathcal{T}_{\upsilon,f}^{\mathrm{FG}} = \frac{\overline{\gamma}_{1,f}}{m_1 2^{\mathcal{R}}}$$

$$P_{SO}^{\mathrm{FSO,VG}} = \frac{(\alpha_e\beta_e)^{\frac{(\alpha_e+\beta_e)}{2}}}{\Gamma(\alpha_e)\Gamma(\beta_e)\overline{\gamma}_{e,o}^{\frac{\alpha_e+\beta_e}{4}}}\Bigg[C_0(1)\sum_{\ell=0}^{m_1-1} C_1(1) \sum_{k=0}^{m_1-\ell-1} A_1 \mathcal{T}_{1,o}^{\mathrm{VG}} + C_0(2)\sum_{\ell=0}^{m_2-1} C_1(2) \sum_{k=0}^{m_2-\ell-1} A_2 \mathcal{T}_{2,o}^{\mathrm{VG}} - C_0(1)C_0(2)\sum_{\ell=0}^{m_1-1} C_1(1)\sum_{\ell=0}^{m_2-1} C_1(2) \sum_{k=0}^{m_1+m_2-2\ell-2} A_3 \mathcal{T}_{3,o}^{\mathrm{VG}}\Bigg]. \tag{77}$$

$$P_{SO}^{\mathrm{RF,VG}} = \frac{m_e^{m_e}}{\Gamma(m_e)\overline{\gamma}_{e,f}^{m_e}}\Bigg[C_0(1)\sum_{\ell=0}^{m_1-1} C_1(1) \sum_{k=0}^{m_1-\ell-1} A_1 \mathcal{T}_{1,f}^{\mathrm{VG}} + C_0(2)\sum_{\ell=0}^{m_2-1} C_1(2) \sum_{k=0}^{m_2-\ell-1} A_2 \mathcal{T}_{2,f}^{\mathrm{VG}} - C_0(1)C_0(2)\sum_{\ell=0}^{m_1-1} C_1(1)\sum_{\ell=0}^{m_2-1} C_1(2) \sum_{k=0}^{m_1+m_2-2\ell-2} A_3 \mathcal{T}_{3,f}^{\mathrm{VG}}\Bigg], \tag{78}$$

$$P_{SO}^{\mathrm{HYB,VG}} = C_0(e)\sum_{\ell=0}^{m_e-1} C_1(e)\Bigg[C_0(1)\sum_{\ell=0}^{m_1-1} C_1(1) \sum_{k=0}^{m_1-\ell-1} A_1\left((m_e-\ell-2)\mathcal{T}_{1,h}^{\mathrm{VG}} - \frac{m_e}{\overline{\gamma}_{e,f}}\mathcal{T}_{2,h}^{\mathrm{VG}}\right) + C_0(2)\sum_{\ell=0}^{m_2-1} C_1(2) \sum_{k=0}^{m_2-\ell-1} A_2\left((m_e-\ell-2)\mathcal{T}_{3,h}^{\mathrm{VG}} - \frac{m_e}{\overline{\gamma}_{e,f}}\mathcal{T}_{4,h}^{\mathrm{VG}}\right) - C_0(1)C_0(2)\sum_{\ell=0}^{m_1-1} C_1(1)\sum_{\ell=0}^{m_2-1} C_1(2) \sum_{k=0}^{m_1+m_2-2\ell-2} A_3\left((m_e-\ell-2)\mathcal{T}_{5,h}^{\mathrm{VG}} - \frac{m_e}{\overline{\gamma}_{e,f}}\mathcal{T}_{6,h}^{\mathrm{VG}}\right)\Bigg]. \tag{79}$$

$$\times G_{0,1:0,2:0,1}^{1,0:2,0:1,0}\left(\begin{matrix}a_1+1\\-\end{matrix}\middle|\begin{matrix}-,-\\a_2,a_2\end{matrix}\middle|\begin{matrix}-,-\\m_e-1\end{matrix}\middle|\frac{\mathcal{G}m_2}{\overline{\gamma}_{2,f}},\frac{\alpha_e\beta_e\overline{\gamma}_{1,f}}{m_1 2^{\mathcal{R}}\sqrt{\overline{\gamma}_{e,o}}}\right), \tag{83}$$

where $\upsilon \in \{1, 2\}$, and the parameters a_1 and a_2 are given in Appendix with (103).

6) HYBRID EAVESDROPPER FOR FIXED-GAIN

For the hybrid-type eavesdropper considering FG relay scheme, the PDF of SNR $f_{\gamma_e}(\gamma_e)$ is given in (25). Therefore, by substituting (25) and (35) into (70), the lower bound of SOP is obtained as (88), shown at the bottom of the page, in terms of $\mathcal{T}_{1,h}^{\mathrm{VG}}$, $\mathcal{T}_{2,h}^{\mathrm{VG}}$, $\mathcal{T}_{3,h}^{\mathrm{VG}}$ and $\mathcal{T}_{4,h}^{\mathrm{VG}}$.

Since $\mathcal{T}_{1,h}^{\mathrm{VG}}$, $\mathcal{T}_{2,h}^{\mathrm{VG}}$, $\mathcal{T}_{3,h}^{\mathrm{VG}}$ and $\mathcal{T}_{4,h}^{\mathrm{VG}}$ are in the same form with different parameters, their derivations can be made as

$$\mathcal{T}_{\upsilon,h}^{\mathrm{HYB}} = \int_0^\infty G_{0,1}^{1,0}\left(\frac{m_e}{\overline{\gamma}_{e,f}}\gamma_e\middle|\begin{matrix}-\\a_3\end{matrix}\right) G_{0,1}^{1,0}\left(\frac{m_1 2^{\mathcal{R}}}{\overline{\gamma}_{1,f}}\gamma_e\middle|\begin{matrix}-\\a_1\end{matrix}\right) \times G_{0,2}^{2,0}\left(\frac{\mathcal{G}m_1 m_2 2^{\mathcal{R}}}{\overline{\gamma}_{1,f}\overline{\gamma}_{2,f}}\gamma_e\middle|\begin{matrix}-,-\\a_2,a_2\end{matrix}\right)\cdot d\gamma_e, \tag{84}$$

and the resultant integral can be solved in terms of EGBMG function by using [85, (20)]

$$\mathcal{T}_{\upsilon,h}^{\mathrm{FG}} = \frac{\overline{\gamma}_{1,f}}{m_1 2^{\mathcal{R}}} \times G_{0,1:0,1:0,2}^{1,0:1,0:2,0}\left(\begin{matrix}a_1+1\\-\end{matrix}\middle|\begin{matrix}-\\a_3\end{matrix}\middle|\begin{matrix}-,-\\a_2,a_2\end{matrix}\middle|\frac{m_e\overline{\gamma}_{1,f}}{m_1 2^{\mathcal{R}}\sqrt{\overline{\gamma}_{e,f}}},\frac{\mathcal{G}m_2}{\overline{\gamma}_{2,f}}\right), \tag{85}$$

where $\upsilon \in \{1, 2, 3, 4\}$, and the parameters a_1, a_2 and a_3 are given in Appendix with (104).

C. EFFECTIVE SECRECY THROUGHPUT

The effective secrecy throughput, denoted by T_{Eff}, is a metric used to evaluate the throughput of a system based on the secrecy outage probability. It is given as [51]

$$T_{ES} = \mathcal{R} \times \big(1 - P_{SO}(\mathcal{R})\big). \tag{89}$$

1) VARIABLE-GAIN RELAYING

For the VG AF relaying scheme, the effective throughput is calculated by using SOP metric for FSO, RF and hybrid eavesdroppers, respectively, given as

$$T_{ES}^{\mathrm{FSO,VG}}(\mathcal{R}) = \mathcal{R} \times \big(1 - P_{SO}^{\mathrm{FSO,VG}}(2^{\mathcal{R}} - 1)\big), \tag{90}$$
$$T_{ES}^{\mathrm{RF,VG}}(\mathcal{R}) = \mathcal{R} \times \big(1 - P_{SO}^{\mathrm{RF,VG}}(2^{\mathcal{R}} - 1)\big), \tag{91}$$
$$T_{ES}^{\mathrm{HYB,VG}}(\mathcal{R}) = \mathcal{R} \times \big(1 - P_{SO}^{\mathrm{HYB,VG}}(2^{\mathcal{R}} - 1)\big), \tag{92}$$

where $P_{SO}^{\mathrm{FSO,VG}}$, $P_{SO}^{\mathrm{RF,VG}}$ and $P_{SO}^{\mathrm{HYB,VG}}$ denote the SOP, as given in (77), (78) and (79), respectively.

2) FIXED-GAIN RELAYING

For FG AF relaying scheme, the effective throughput is expressed using the lower bound of SOP metric for FSO, RF and hybrid eavesdroppers, respectively, given as

$$T_{ES_L}^{\mathrm{FSO,FG}}(\mathcal{R}) = \mathcal{R} \times \big(1 - P_{SO_L}^{\mathrm{FSO,FG}}(2^{\mathcal{R}} - 1)\big), \tag{93}$$
$$T_{ES_L}^{\mathrm{RF,FG}}(\mathcal{R}) = \mathcal{R} \times \big(1 - P_{SO_L}^{\mathrm{RF,FG}}(2^{\mathcal{R}} - 1)\big), \tag{94}$$
$$T_{ES_L}^{\mathrm{HYB,FG}}(\mathcal{R}) = \mathcal{R} \times \big(1 - P_{SO_L}^{\mathrm{HYB,FG}}(2^{\mathcal{R}} - 1)\big), \tag{95}$$

where $P_{SO_L}^{\mathrm{FSO,FG}}$, $P_{SO_L}^{\mathrm{RF,FG}}$ and $P_{SO_L}^{\mathrm{HYB,FG}}$ denote the lower bound of SOP, as given in (86), (87) and (88), respectively.

V. RESULTS AND DISCUSSION

This section is dedicated for detailed characterization of the secrecy performance of the considered dual-hop relaying hybrid FSO-*mm*Wave systems in the presense of the considered three type of the eavesdroppers. Specifically, the accuracy of the analytical formulas derived in Section IV are validated through Monte Carlo simulations. Both analytical and simulation results depict the physical layer security performance in terms of the average secrecy capacity, secrecy outage probability and effective secrecy throughput. The results provided in this section include various scenarios with several fundamental physical layer parameters such as average SNRs, link distances, fraction of received power, weather conditions, and relaying schemes. The simulation parameters of the system and channel models are given in

$$P_{SO_L}^{\mathrm{FSO,FG}} = \frac{(\alpha_e\beta_e)^{\frac{(\alpha_e+\beta_e)}{2}}}{\Gamma(\alpha_e)\Gamma(\beta_e)\overline{\gamma}_{e,o}^{\frac{\alpha_e+\beta_e}{4}}} C_0(1)\sum_{\ell_1=0}^{m_1-1} C_1(1)C_0(2)\sum_{\ell_2=0}^{m_2-1} C_1(2)\sum_{k=0}^{m_1-\ell_1-1} B_1\left[\widehat{B}_2\mathcal{T}_{1,o}^{\mathrm{FG}} - \widehat{B}_3\mathcal{T}_{2,o}^{\mathrm{FG}}\right], \tag{86}$$

$$P_{SO_L}^{\mathrm{RF,FG}} = \frac{m_e^{m_e}}{\Gamma(m_e)\overline{\gamma}_{e,f}^{m_e}}\left(\frac{m_e}{\overline{\gamma}_{e,f}}\right)^{-(m_e-1)} C_0(1)\sum_{\ell_1=0}^{m_1-1} C_1(1)C_0(2)\sum_{\ell_2=0}^{m_2-1} C_1(2)\sum_{k=0}^{m_1-\ell_1-1} B_1\left[\widehat{B}_2\mathcal{T}_{1,f}^{\mathrm{FG}} - \widehat{B}_3\mathcal{T}_{2,f}^{\mathrm{FG}}\right], \tag{87}$$

$$P_{SO_L}^{\mathrm{HYB,FG}} = C_0(e)\sum_{\ell=0}^{m_e-1} C_1(e)C_0(1)\sum_{\ell_1=0}^{m_1-1} C_1(1)C_0(2)\sum_{\ell_2=0}^{m_2-1} C_1(2)\sum_{k=0}^{m_1-\ell_1-1} B_1\left(\frac{m_e}{\overline{\gamma}_{e,f}}\right)^{-(m_e-\ell-1)} \times\left[(m_e-\ell-2)\left(\frac{m_e}{\overline{\gamma}_{e,f}}\right)^{-(m_e-\ell-2)}\left(\widehat{B}_2\mathcal{T}_{1,h}^{\mathrm{FG}} - \widehat{B}_3\mathcal{T}_{3,h}^{\mathrm{FG}}\right) - \widehat{B}_2\mathcal{T}_{2,h}^{\mathrm{FG}} + \widehat{B}_3\mathcal{T}_{4,h}^{\mathrm{FG}}\right]. \tag{88}$$

TABLE 1. Physical layer parameters of FSO and *mm*Wave systems.

FSO System		
Parameters	*Symbols*	*Values*
Wavelength	λ_o	1550 mm
Optical Power	I_t	40 mW
Aperture's Diameter	A	0.2 m
Beam Divergence	ψ	10 mrad
Photosensitivity	ξ	0.5 A/W
***m*mWave System**		
Parameters	*Symbols*	*Values*
Wavelength	λ_f	$c/60$ nm
Electrical Power	P_t	10 mW
Transmitter Antenna Gain	G_T	44 dBi
Receiver Antenna Gain	G_R	44 dBi
Oxygen Absorption	φ_{O_2}	15.1 dB/km

* c is the speed of light.

TABLE 2. Parameters for different weather conditions.

Weather-Dependent Parameters			
Weather Conditions	υ_o *(dB/km)*	φ_{rain} *(dB/km)*	C_n^2
Clean Air	0.43	0	5×10^{-14}
Haze	4.2	0	1.7×10^{-14}
Moderate Rain (12.5 mm/h)	5.8	5.6	5×10^{-15}

Table 1 and Table 2 [73], [74], [86]. It worth highlighting here that, in the explored results for different scenarios and configurations, the average electrical SNR of each link is assumed to be equal, which is controlled by setting the electrical transmit power at the *mm*Wave link to a specific value, and calculating the corresponding optical transmit power and noise power values. Also, the computation of EGBMG function included in the analytical results has been performed with the code generated in [87].

Fig. 2 depicts the secrecy capacity analysis versus the average SNR of the first hop (or the second hop) of the considered dual-hop hybrid FSO-RF relaying system considering different types of eavesdroppers. The secrecy performance of both FG and VG AF relaying schemes is conducted in clean weather conditions, where the distances d_1 and d_2 are set to 1 km and 1.25 km, respectively. Also, the gain $\mathcal{G}$ is set to 0.5 for FG relaying scheme, and the average SNR at Eve is adjusted as $\overline{\gamma}_e = 5$ dB. As the turbulence parameters are distance dependant, the pairs of turbulence parameters are different between the two hops. Specifically, they are estimated as ($\alpha_1 = 5.0096, \beta_1 = 4.7489$) and ($\alpha_2 = 4.2937, \beta_2 = 4.0462$), where the Nakagami-$m$ parameter is set to $m_1 = m_2 = 1$. As shown, the FG scheme performs better than the VG, since FG scheme exploits the full channel state information. Additionally, it can be observed that the hybrid-type eavesdropper can severely impact the secrecy capacity for both FG and VG relaying schemes, with respect to both FSO- and RF-Eves. For instance, considering a fixed SNRs of 8 dB, the achievable average secrecy capacities are approximately 2.5, 1.8, 1 bits for VG scheme in the presence of FSO-, RF- and hybrid eavesdroppers, respectively, where these values are 4.4, 4, 3.7 bits for FG relaying scheme.

Since a hybrid eavesdropper has the most severe impact on the secrecy performance among other types, the secrecy capacity of the dual-hop hybrid system is investigated as a function of the link distances in the presence of a hybrid

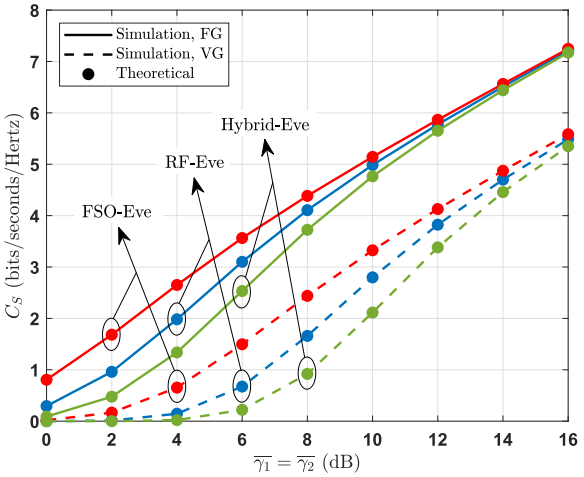

FIGURE 2. Average secrecy capacity as a function of the average SNR for different types of eavesdroppers. (Clean weather, $\mathcal{G} = 0.5$, $d_1 = 1$ km, $d_2 = d_e = 1.25$ km $m_1 = m_2 = 1$, $\alpha_1 = 5.01$, $\beta_1 = 4.74$, $\alpha_2 = \alpha_e = 4.29$, $\beta_2 = \beta_e = 4.04$, $R_{1,o} = R_{1,f} = 0.8$, $R_{2,o} = R_{2,f} = 0.7$, $R_{e,o} = R_{e,f} = 0.2$, $\overline{\gamma}_e = 5$ dB).

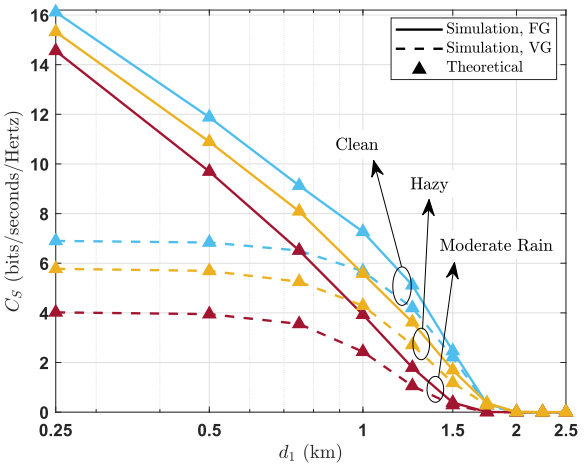

FIGURE 3. Average secrecy capacity as a function of the distance of first-hop in the presence of a hybrid-type Eve for different weather conditions. ($\mathcal{G} = 0.5$, $d_2 = d_e = 1$ km, $m_1 = m_2 = 1$, $\alpha_2 = \alpha_e = 6.91$, $\beta_2 = \beta_e = 6.59$, $R_{1,o} = R_{1,f} = R_{2,o} = R_{2,f} = 0.75$, $R_{e,o} = R_{e,f} = 0.2$, $\overline{\gamma}_1 = \overline{\gamma}_2 = 15$ dB, $\overline{\gamma}_e = 3$ dB).

Eve. Fig. 3 and Fig. 4 explore impact of different weather conditions on the security performance for both FG and VG relaying schemes at the fixed SNRs of $\overline{\gamma}_1 = \overline{\gamma}_2 = 15$ dB, and $\overline{\gamma}_e = 3$ dB. The link distance d_2 is set to 1 km in Fig. 3, while d_1 is set to 1 km in Fig. 4. It can be observed that the weather conditions have a significant impact on the system's secrecy capacity for both FG and VG relaying techniques. Specifically, When the weather conditions vary from clean to moderate rain, the transmission reliability decreases significantly. For instance, in Fig. 3, considering a link distance of $d_1 = 1$ km, the expected secrecy capacity values are approximately 2.5, 4.2 and 5.9 bits for moderate rain, hazy and clean weather conditions, respectively. These numbers are, in turn, approximately 4, 5.9 and 7.4 bits for FG relaying scheme. Furthermore, one can easily observe the saturated behavior of the capacity curves in Fig. 3, which is because

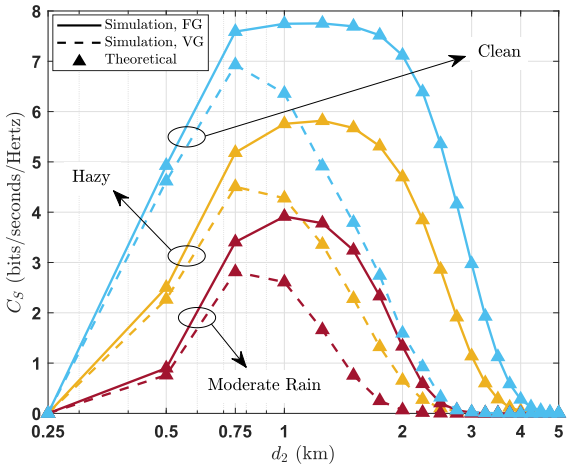

FIGURE 4. Average secrecy capacity as a function of the distance of second-hop in the presence of a hybrid-type Eve for different weather conditions. ($\mathcal{G} = 0.5$, $d_1 = 1$ km, $d_e = d_2$, $m_1 = m_2 = 1$, $\alpha_1 = 6.91$, $\beta_1 = 6.59$, $R_{1,o} = R_{1,f} = R_{2,o} = R_{2,f} = 0.75$, $R_{e,o} = R_{e,f} = 0.2$, $\overline{\gamma}_1 = \overline{\gamma}_2 = 15$ dB, $\overline{\gamma}_e = 3$ dB).

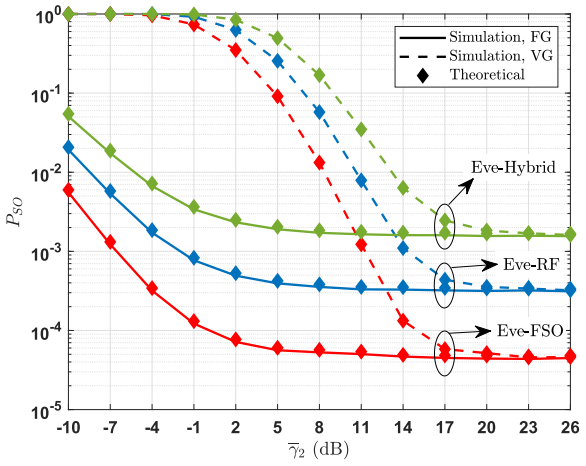

FIGURE 5. Secrecy outage probability as a function of average SNR at second-hop for different types of eavesdroppers. (Hazy weather, $\mathcal{G} = 0.5$, $\mathcal{R} = 2$ bits, $d_1 = d_2 = d_e = 1.5$ km, $m_1 = m_2 = 1$, $\alpha_1 = \alpha_2 = \alpha_e = 3.02$, $\beta_1 = \beta_2 = \beta_e = 2.71$, $R_{1,o} = R_{1,f} = R_{2,o} = R_{2,f} = 0.65$, $R_{e,o} = R_{e,f} = 0.15$, $\overline{\gamma}_1 = 11$ dB, $\overline{\gamma}_e = 3$ dB).

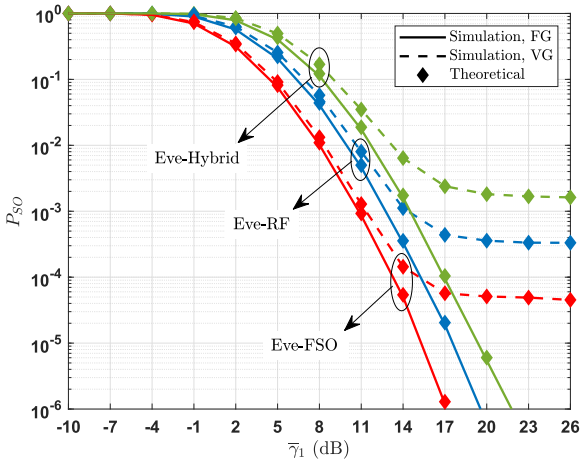

FIGURE 6. Secrecy outage probability as a function of average SNR at first-hop for different types of eavesdroppers. (Hazy weather, $\mathcal{G} = 0.5$, $\mathcal{R} = 2$ bits, $d_1 = d_2 = d_e = 1.5$ km, $m_1 = m_2 = 1$, $\alpha_1 = \alpha_2 = \alpha_e = 3.02$, $\beta_1 = \beta_2 = \beta_e = 2.71$, $R_{1,o} = R_{1,f} = R_{2,o} = R_{2,f} = 0.65$, $R_{e,o} = R_{e,f} = 0.15$, $\overline{\gamma}_2 = 11$ dB, $\overline{\gamma}_e = 3$ dB).

of the limited average SNR in the second-hop. On the other hand, limiting the average SNR in the first-hop results in a non-monotonic capacity performance.

In Fig. 5, the secrecy outage probability of the considered system is plotted versus the average SNR of the second hop at a fixed SNR of the first hope ($\overline{\gamma_1}$ =11 dB), while Fig. 6 considers the secrecy outage probability versus the average SNR of the first hop at a fixed SNR of the second hop ($\overline{\gamma_2}$ =11 dB). In both figures, the impact of different types of eavesdroppers on the secrecy outage probability is explored for both FG and VG relaying schemes considering $d_1 = d_2$ =1.5 km, a fixed SNR of $\overline{\gamma}_e = 3$ dB at Eve, and the outage threshold is set to $\mathcal{R} = 2$ bits. As clearly shown, different Eve types have different impacts on the system's secrecy outage probability for both relaying schemes. For instance, in Fig. 5, considering a fixed average SNR of $\overline{\gamma}_2 = 11$ dB, the expected outage probabilities are 5×10^{-5}, 4×10^{-4} and 2×10^{-3} for FSO-, RF- and hybrid type eavesdroppers, respectively, with FG scheme. These number are, in turn, approximately 9×10^{-2}, 3×10^{-1} and 7×10^{-1} for VG relaying scheme. Moreover, another important observation can be made from Figs. 5 and 6, where the impact of the average SNR in the first-hop for FG AF relaying scheme is clearly shown. The average SNR of the first hop can significantly enhance the secrecy outage probability of the FG relaying scheme. It is mainly due to the fact that amplification directly depends on the received SNR at the relay node, which allows the SNR of first-hop to have an important role on the SOP for FG scheme. For instance, fixing the SNR in the first-hop leads to flooring the SOP curve, which yields in a saturation in the reliability, and therefore, the outage performance cannot be improved beyond a specific level. On the other hand, varying the SNR in the first-hop and fixing the SNR in the second-hop does not lead to the same result for FG but for VG AF relaying scheme. This is mainly due to the fact that VG scheme always adopts the lowest SNR in the two hops.

The secrecy outage performance of the dual-hop hybrid system as a function of the outage threshold is illustrated in the presence of different types of eavesdroppers for FG and VF AF relaying schemes. The weather conditions are considered as clean, and the distances in each link assumed as $d_1 = d_2 = d_e = 2$ km, while the average fixed SNRs is set to $\overline{\gamma}_1 = \overline{\gamma}_2 = 10$ dB, and $\overline{\gamma}_e = 3$ dB. Accordingly, the optical channel parameters are calculated as $\alpha_1 = \alpha_2 = \alpha_e = 3.31$, and $\beta_1 = \beta_2 = \beta_e = 2.58$, where the Nakagami-$m$ parameters are set to $m_1 = m_2 = 1$. As expected, increasing the outage threshold decreases the secrecy performance, however, the average throughput also increases as a tradeoff.

A final result regarding the effective secrecy throughput metric is illustrated in Fig. 8, which is plotted versus the outage threshold $\mathcal{R}$ for the considered system in the presence of different types of eavesdroppers. The distances d_1

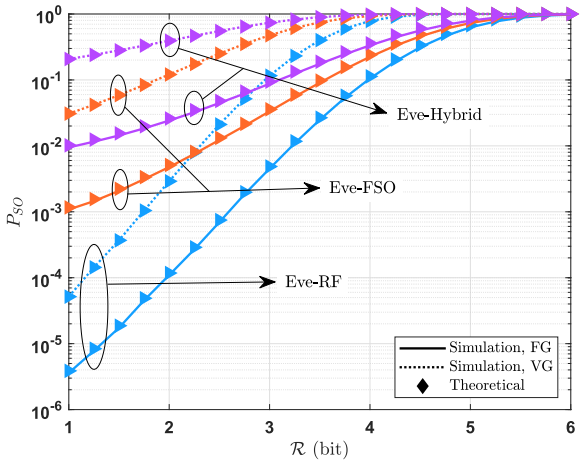

FIGURE 7. Secrecy outage probability as a function of threshold value for different types of eavesdroppers. (Clean weather, $\mathcal{G} = 0.5$, $d_1 = d_2 = d_e = 2$ km, $m_1 = m_2 = 1$, $\alpha_1 = \alpha_2 = \alpha_e = 3.31$, $\beta_1 = \beta_2 = \beta_e = 2.58$, $R_{1,o} = R_{1,f} = R_{2,o} = R_{2,f} = 0.65$, $R_{e,o} = R_{e,f} = 0.25$, $\overline{\gamma}_1 = \overline{\gamma}_2 = 10$ dB, $\overline{\gamma}_e = 3$ dB).

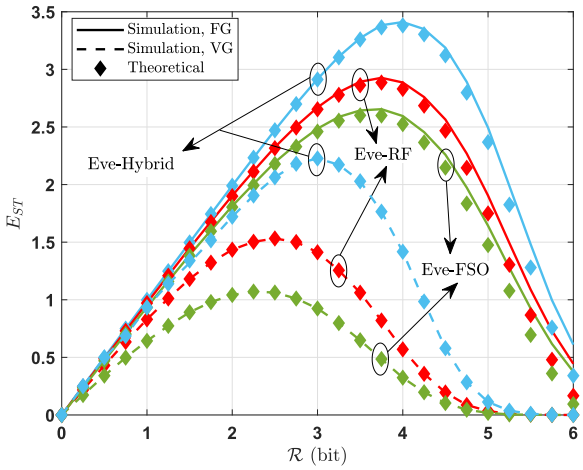

FIGURE 8. Effective secrecy throughput as a function of threshold value for different types of eavesdroppers. (Moderate-rainy weather, $\mathcal{G} = 0.5$, $m_1 = m_2 = 1$, $\alpha_1 = \alpha_2 = \alpha_e = 2.98$, $\beta_1 = \beta_2 = \beta_e = 2.52$, $R_{1,o} = R_{1,f} = R_{2,o} = R_{2,f} = 0.75$, $R_{e,o} = R_{e,f} = 0.25$, $d_1 = d_2 = 1.75$ km, $\overline{\gamma}_1 = \overline{\gamma}_2 = 12$ dB, $d_e = 1.75$ km, $\overline{\gamma}_e = 5$ dB).

and d_2 are assumed identical and equal to 1.75 km, while the Nakagami-m parameters are set to $m_1 = m_2 = 1$ in both hops. Additionally, the turbulence parameters are calculated as $\alpha_1 = \alpha_2 = \alpha_e = 2.9846$, and $\beta_1 = \beta_2 = \beta_e = 2.5254$. From the figure, the expected convex curves of the effective secrecy throughput T_{ES} for the different types of Eve and both FG and VG relaying schemes. At low values of $\mathcal{R}$, the dominant impact is related to threshold it self $\mathcal{R}$ which results in increasing the T_{ES}. However, after exceeding a specific value of $\mathcal{R}$, the secrecy outage probability becomes dominant, which negatively affects T_{ES} resulting in the convex shape shown in Fig. 8.

VI. CONCLUSION

This article addresses the secrecy performance of dual-hop hybrid FSO-*mm*Wave systems where both FSO and *mm*Wave links are simultaneously used at each hop. A set of different types of eavesdroppers are considered based on the eavesdropper's ability and resources. The analysis conducted in this work have led to obtaining mathematical expressions of different secrecy metrics such as secrecy capacity, secrecy outage probability and effective secrecy throughput. In all analysis, the Gamma-Gamma model has been used to describe the weather turbulence for the FSO link, and Nakagami-m to model the small-scale fading in *mm*Wave link. Moreover, two different AF relaying scheme have been taken into account, namely fixed and variable gain relaying. Obtained results have revealed that hybrid-type eavesdropper can severely impact the secrecy performance as compared other types, i.e., FSO- and RF-Eves. According to the performance results extracted, dual-hop hybrid FSO-*mm*Wave system should be nominated as good candidate to design back-haul systems with improved reliability and spectral efficiency. For Future work, the asymptotic secrecy analysis of the dual-hop hybrid FSO-*mm*Wave system will be investigated along with considering more practical scenarios such as the pointing errors in FSO link and misalignment in *mm*Wave link and their impact on the overall secrecy performance.

APPENDIX
DEFINITION OF THE PARAMETERS

The parameters a_1 and a_2 that are used in (44) and (51)

$$\begin{cases} a_1 = m_1 - \ell - 1, \\ a_2 = m_1/\overline{\gamma}_{1,f}, \end{cases} \text{for } \mathcal{I}^{\text{VG}}_{2,o}, \text{ and } \mathcal{I}^{\text{VG}}_{2,f},$$
$$\begin{cases} a_1 = m_2 - \ell - 1, \\ a_2 = m_2/\overline{\gamma}_{2,f}, \end{cases} \text{for } \mathcal{I}^{\text{VG}}_{3,o}, \text{ and } \mathcal{I}^{\text{VG}}_{3,f},$$
$$\begin{cases} a_1 = m_1 + m_2 - 2\ell - 2, \\ a_2 = m_1/\overline{\gamma}_{1,f} + m_2/\overline{\gamma}_{2,f}, \end{cases} \text{for } \mathcal{I}^{\text{VG}}_{4,o}, \text{ and } \mathcal{I}^{\text{VG}}_{4,f}. \quad (96)$$

The parameters a_1 and a_2 that are used in (53)

$$\begin{cases} a_1 = m_e - \ell_e - 1, \\ a_2 = m_e/\overline{\gamma}_{e,f}, \end{cases} \text{for } \mathcal{I}^{\text{VG}}_{1,h},$$
$$\begin{cases} a_1 = m_1 + m_e - \ell - \ell_e - 2, \\ a_2 = m_1/\overline{\gamma}_{1,f} + m_e/\overline{\gamma}_{e,f}, \end{cases} \text{for } \mathcal{I}^{\text{VG}}_{2,h},$$
$$\begin{cases} a_1 = m_2 + m_e - \ell - \ell_e - 2, \\ a_2 = m_2/\overline{\gamma}_{2,f} + m_e/\overline{\gamma}_{e,f}, \end{cases} \text{for } \mathcal{I}^{\text{VG}}_{3,h},$$
$$\begin{cases} a_1 = m_1 + m_2 + m_e - 2\ell - \ell_e - 3, \\ a_2 = m_1/\overline{\gamma}_{1,f} + m_2/\overline{\gamma}_{2,f} + m_e/\overline{\gamma}_{e,f}, \end{cases} \text{for } \mathcal{I}^{\text{VG}}_{4,h}. \quad (97)$$

The parameters a_1, a_2, b_1 and b_2 that are used in (59) and (62)

$$\begin{cases} a_1 = (2m_1 + m_2 - 2\ell_1 - \ell_2 - k - 5)/2, \\ a_2 = (m_2 - \ell_2 - k - 2)/2, \\ b_1 = m_1/\overline{\gamma}_{1,f}, \\ b_2 = \mathcal{G} m_1 m_2/\overline{\gamma}_{1,f}\overline{\gamma}_{2,f} \end{cases} \text{for } \mathcal{I}^{\text{FG}}_{2,o} \text{ and } \mathcal{I}^{\text{FG}}_{2,f},$$

$$\begin{cases} a_1 = (2m_1 + m_2 - 2\ell_1 - \ell_2 - k - 3)/2, \\ a_2 = (m_2 - \ell_2 - k - 1)/2, \\ b_1 = m_1/\overline{\gamma}_{1,f}, \\ b_2 = \mathcal{G} m_1 m_2/\overline{\gamma}_{1,f}\overline{\gamma}_{2,f} \end{cases} \text{for } \mathcal{I}^{\text{FG}}_{3,o} \text{ and } \mathcal{I}^{\text{FG}}_{3,f}. \tag{98}$$

The parameters a_1, a_2, b_1 and b_2 that are used in (65)

$$\begin{cases} a_1 = (2m_1 + m_2 + 2m_e - 2\ell_1 - \ell_2 - \ell - k - 7)/2, \\ a_2 = (m_2 - \ell_2 - k - 2)/2, \\ b_1 = (m_1/\overline{\gamma}_{1,f}) + (m_e/\overline{\gamma}_{e,f}), \\ b_2 = \mathcal{G} m_1 m_2/\overline{\gamma}_{1,f}\overline{\gamma}_{2,f} \end{cases} \text{for } \mathcal{I}^{\text{FG}}_{2,h},$$

$$\begin{cases} a_1 = (2m_1 + m_2 + 2m_e - 2\ell_1 - \ell_2 - \ell - k - 5)/2, \\ a_2 = (m_2 - \ell_2 - k - 1)/2, \\ b_1 = (m_1/\overline{\gamma}_{1,f}) + (m_e/\overline{\gamma}_{e,f}), \\ b_2 = \mathcal{G} m_1 m_2/\overline{\gamma}_{1,f}\overline{\gamma}_{2,f} \end{cases} \text{for } \mathcal{I}^{\text{FG}}_{3,h}. \tag{99}$$

The parameters a_1 and a_2 that are used in (72)

$$\begin{cases} a_1 = m_1 - \ell + \dfrac{\alpha_e + \beta_e}{4} - 1, \\ a_2 = m_1(2^{\mathcal{R}} - 1)/\overline{\gamma}_{1,f}, \end{cases} \text{for } \mathcal{I}^{\text{VG}}_{1,o},$$

$$\begin{cases} a_1 = m_2 - \ell + \dfrac{\alpha_e + \beta_e}{4} - 1, \\ a_2 = m_2(2^{\mathcal{R}} - 1)/\overline{\gamma}_{2,f}, \end{cases} \text{for } \mathcal{I}^{\text{VG}}_{2,o},$$

$$\begin{cases} a_1 = m_1 + m_2 - 2\ell + \dfrac{\alpha_e + \beta_e}{4} - 2, \\ a_2 = m_1/\overline{\gamma}_{1,f} + m_2/\overline{\gamma}_{2,f}, \end{cases} \text{for } \mathcal{I}^{\text{VG}}_{3,o}. \tag{100}$$

The parameters a_1 and a_2 that are used in (74)

$$\begin{cases} a_1 = m_1 + m_e - \ell - 2, \\ a_2 = m_1(2^{\mathcal{R}} - 1)/\overline{\gamma}_{1,f} + m_e/\overline{\gamma}_{e,f}, \end{cases} \text{for } \mathcal{I}^{\text{VG}}_{1,f},$$

$$\begin{cases} a_1 = m_2 + m_e - \ell - 2, \\ a_2 = m_2(2^{\mathcal{R}} - 1)/\overline{\gamma}_{2,f} + m_e/\overline{\gamma}_{e,f}, \end{cases} \text{for } \mathcal{I}^{\text{VG}}_{2,f},$$

$$\begin{cases} a_1 = m_1 + m_2 + m_e - 2\ell - 3, \\ a_2 = (m_1/\overline{\gamma}_{1,f} + m_2/\overline{\gamma}_{2,f})2^{\mathcal{R}} + m_e/\overline{\gamma}_{e,f}, \end{cases} \text{for } \mathcal{I}^{\text{VG}}_{3,f}. \tag{101}$$

The parameters a_1 and a_2 that are used in (76)

$$\begin{cases} a_1 = m_1 + m_e - 2\ell - 4, \\ a_2 = m_1(2^{\mathcal{R}} - 1)/\overline{\gamma}_{1,f} + m_e/\overline{\gamma}_{e,f}, \end{cases} \text{for } \mathcal{I}^{\text{VG}}_{1,h},$$

$$\begin{cases} a_1 = m_1 + m_e - 2\ell - 3, \\ a_2 = m_1(2^{\mathcal{R}} - 1)/\overline{\gamma}_{1,f} + m_e/\overline{\gamma}_{e,f}, \end{cases} \text{for } \mathcal{I}^{\text{VG}}_{4,h},$$

$$\begin{cases} a_1 = m_2 + m_e - 2\ell - 4, \\ a_2 = m_2(2^{\mathcal{R}} - 1)/\overline{\gamma}_{2,f} + m_e/\overline{\gamma}_{e,f}, \end{cases} \text{for } \mathcal{I}^{\text{VG}}_{2,h},$$

$$\begin{cases} a_1 = m_2 + m_e - 2\ell - 3, \\ a_2 = m_2(2^{\mathcal{R}} - 1)/\overline{\gamma}_{2,f} + m_e/\overline{\gamma}_{e,f}, \end{cases} \text{for } \mathcal{I}^{\text{VG}}_{5,h},$$

$$\begin{cases} a_1 = m_1 + m_2 + m_e - 2\ell - 5, \\ a_2 = (m_1/\overline{\gamma}_{1,f} + m_2/\overline{\gamma}_{2,f})2^{\mathcal{R}} + m_e/\overline{\gamma}_{e,f}, \end{cases} \text{for } \mathcal{I}^{\text{VG}}_{3,h},$$

$$\begin{cases} a_1 = m_1 + m_2 + m_e - 2\ell - 4, \\ a_2 = (m_1/\overline{\gamma}_{1,f} + m_2/\overline{\gamma}_{2,f})2^{\mathcal{R}} + m_e/\overline{\gamma}_{e,f}, \end{cases} \text{for } \mathcal{I}^{\text{VG}}_{6,h}. \tag{102}$$

The parameters a_1 and a_2 that are used in (81) and (83)

$$\begin{cases} a_1 = (2m_1 + m_2 - 2\ell_1 - \ell_2 - k - 5)/2, \\ a_2 = (m_2 - \ell_2 - k - 2)/2, \end{cases} \text{for } \mathcal{I}^{\text{FG}}_{1,o},$$

$$\begin{cases} a_1 = (2m_1 + m_2 - 2\ell_1 - \ell_2 - k - 3)/2, \\ a_2 = (m_2 - \ell_2 - k - 1)/2, \end{cases} \text{for } \mathcal{I}^{\text{FG}}_{2,o}. \tag{103}$$

The parameters a_1 and a_2 that are used in (85)

$$\begin{cases} a_1 = (2m_1 + m_2 - 2\ell_1 - \ell_2 - k - 5)/2, \\ a_2 = (m_2 - \ell_2 - k - 2)/2, \\ a_3 = m_e - \ell - 3, \end{cases} \text{for } \mathcal{I}^{\text{FG}}_{1,h},$$

$$\begin{cases} a_1 = (2m_1 + m_2 - 2\ell_1 - \ell_2 - k - 3)/2, \\ a_2 = (m_2 - \ell_2 - k - 1)/2, \\ a_3 = m_e - \ell - 3, \end{cases} \text{for } \mathcal{I}^{\text{FG}}_{2,h},$$

$$\begin{cases} a_1 = (2m_1 + m_2 - 2\ell_1 - \ell_2 - k - 5)/2, \\ a_2 = (m_2 - \ell_2 - k - 2)/2, \\ a_3 = m_e - \ell - 2, \end{cases} \text{for } \mathcal{I}^{\text{FG}}_{3,h},$$

$$\begin{cases} a_1 = (2m_1 + m_2 - 2\ell_1 - \ell_2 - k - 3)/2, \\ a_2 = (m_2 - \ell_2 - k - 1)/2, \\ a_3 = m_e - \ell - 2, \end{cases} \text{for } \mathcal{I}^{\text{FG}}_{4,h}. \tag{104}$$

The parameters B_1, B_2, and B_3 that are used in (34), (35), (66), (67), (68), (86), (87), and (88)

$$\begin{aligned} B_1 &= \binom{m_1 - \ell_1 - 1}{k} \mathcal{G}^k \left(\frac{\mathcal{G} m_1 \overline{\gamma}_{2,f}}{m_2 \overline{\gamma}_{1,f}} \right)^{\frac{m_2 - \ell_2 - k - 1}{2}}, \\ B_2 &= (m_2 - \ell_2 - 2) m_2 \overline{\gamma}_{1,f} / \mathcal{G} m_1 \overline{\gamma}_{2,f}, \\ B_3 &= m_2/\overline{\gamma}_{2,f}. \end{aligned} \tag{105}$$

The parameters $\widehat{B}_2$ and $\widehat{B}_3$ that are used in (35) (86), (87), and (88)

$$\begin{aligned} \widehat{B}_2 &= \frac{(m_2 - \ell_2 - 2) m_2 \overline{\gamma}_{1,f}}{\mathcal{G} m_1 \overline{\gamma}_{2,f}} \left(\frac{\overline{\gamma}_{1,f}\overline{\gamma}_{2,f}}{\mathcal{G} m_1 m_2} \right)^{\frac{2m_1 + m_2 - 2\ell_1 - \ell_2 - k - 5}{2}}, \\ \widehat{B}_3 &= \frac{m_2}{\overline{\gamma}_{2,f}} \left(\frac{\mathcal{G} m_1 m_2}{\overline{\gamma}_{1,f}\overline{\gamma}_{2,f}} \right)^{-\frac{2m_1 + m_2 - 2\ell_1 - \ell_2 - k - 5}{2}}. \end{aligned} \tag{106}$$

The parameters A_1, A_2, and A_3 that are used in (77), (78), and (79)

$$A_1 = \binom{m_1 - \ell - 1}{k} (2^{\mathcal{R}} - 1)^k 2^{\mathcal{R}(m_1 - \ell - 1)} e^{-\frac{m_1(2^{\mathcal{R}} - 1)}{\overline{\gamma}_{1,f}}},$$

$$A_2 = \binom{m_2 - \ell - 1}{k}(2^{\mathcal{R}} - 1)^k 2^{\mathcal{R}(m_2-\ell-1)} e^{-\frac{m_2(2^{\mathcal{R}}-1)}{\overline{\gamma}_{2,f}}},$$
$$A_3 = \binom{m_1 + m_2 - 2\ell - 2}{k}(2^{\mathcal{R}} - 1)^k 2^{\mathcal{R}(m_1+m_2-2\ell-2)} \times e^{-\left(\frac{m_1}{\overline{\gamma}_{1,f}} + \frac{m_2}{\overline{\gamma}_{2,f}}\right)(2^{\mathcal{R}}-1)}. \quad (107)$$

ACKNOWLEDGMENT

This publication was made possible by NPRP13S-0130-200200 from the Qatar National Research Fund (a member of The Qatar Foundation). The statements made herein are solely the responsibility of the author[s].

REFERENCES

[1] M. Z. Chowdhury, M. Shahjalal, S. Ahmed, and Y. M. Jang, "6G wireless communication systems: Applications, requirements, technologies, challenges, and research directions," *IEEE Open J. Commun. Soc.*, vol. 1, pp. 957–975, 2020.

[2] A. Kliks, L. Kulacz, P. Kryszkiewicz, H. Bogucka, M. Dryjanski, M. Isaksson, G. P. Koudouridis, and P. Tengkvist, "Beyond 5G: Big data processing for better spectrum utilization," *IEEE Veh. Technol. Mag.*, vol. 15, no. 3, pp. 40–50, Sep. 2020.

[3] World Wireless Research Forum. (Nov. 2017). *Wireless Comminication Using Higher Frequency Bands*. [Online]. Available: https://www.wwrf.ch/files/content%20wwrf/publications/outlook/Outlook23.pdf

[4] Y. Wang, J. Li, L. Huang, Y. Jing, A. Georgakopoulos, and P. Demestichas, "5G mobile: Spectrum broadening to higher-frequency bands to support high data rates," *IEEE Veh. Technol. Mag.*, vol. 9, no. 3, pp. 39–46, Sep. 2014.

[5] M. A. Khalighi and M. Uysal, "Survey on free space optical communication: A communication theory perspective," *IEEE Commun. Surveys Tuts.*, vol. 16, no. 4, pp. 2231–2258, 4th Quart., 2014.

[6] A. Vavoulas, H. G. Sandalidis, and D. Varoutas, "Weather effects on FSO network connectivity," *J. Opt. Commun. Netw.*, vol. 4, no. 10, pp. 734–740, Oct. 2012.

[7] S. Althunibat, Z. Altarawneh, and R. Mesleh, "Performance analysis of free space optical–based wireless sensor networks using corner cube retroreflectors," *Trans. Emerg. Telecommun. Technol.*, vol. 30, no. 12, Dec. 2019.

[8] Z. Pi and F. Khan, "An introduction to millimeter-wave mobile broadband systems," *IEEE Commun. Mag.*, vol. 49, no. 6, pp. 101–107, Jun. 2011.

[9] O. S. Badarneh and R. Mesleh, "Diversity analysis of simultaneous mmWave and free-space-optical transmission over F-distribution channel models," *IEEE/OSA J. Opt. Commun. Netw.*, vol. 12, no. 11, pp. 324–334, Mar. 2020.

[10] A. Bhowal and R. S. Kshetrimayum, "Relay based hybrid FSO/RF communication with hybrid spatial modulation and transmit source selection," *IEEE Trans. Commun.*, vol. 68, no. 8, pp. 5018–5027, Aug. 2020.

[11] R. Boluda-Ruiz, S. C. Tokgoz, A. García-Zambrana, and K. Qaraqe, "Asymptotic average secrecy rate for MISO free-space optical wiretap channels," in *Proc. IEEE 20th Int. Workshop Signal Process. Adv. Wireless Commun. (SPAWC)*, Jul. 2019, pp. 1–5.

[12] Md. Z. Hassan, Md. J. Hossain, J. Cheng, and V. C. M. Leung, "Joint FSO fronthaul and millimeter-wave access link optimization in cloud small cell networks: A statistical-QoS aware approach," *IEEE Trans. Commun.*, vol. 67, no. 6, pp. 4208–4226, Jun. 2019.

[13] S. Althunibat, O. S. Badarneh, R. Mesleh, and K. Qaraqe, "A hybrid free space optical-millimeter wave cooperative system," *Opt. Commun.*, vol. 453, Dec. 2019, Art. no. 124400.

[14] S. C. Tokgoz, S. Althunibat, S. L. Miller, and K. A. Qaraqe, "Performance analysis of index modulation based link-selection mechanism for hybrid FSO-mmWave systems," *Opt. Commun.*, vol. 479, Jan. 2021, Art. no. 126305.

[15] M. A. Hasabelnaby, H. A. I. Selmy, and M. I. Dessouky, "Joint optimal transceiver placement and resource allocation schemes for redirected cooperative hybrid FSO/mmW 5G fronthaul networks," *J. Opt. Commun. Netw.*, vol. 10, no. 12, pp. 975–990, Dec. 2018.

[16] S. C. Tokgoz, S. Althunibat, and K. Qaraqe, "A link-selection mechanism for hybrid FSO-mmWave systems based on index modulation," in *Proc. IEEE Int. Conf. Commun. (ICC)*, Jun. 2020, pp. 1–7.

[17] S. Sharma, A. S. Madhukumar, and R. Swaminathan, "Effect of pointing errors on the performance of hybrid FSO/RF networks," *IEEE Access*, vol. 7, pp. 131418–131434, 2019.

[18] M. A. Amirabadi and V. Tabataba Vakili, "Performance evaluation of a novel relay-assisted hybrid FSO/RF communication system with receive diversity," *IET Optoelectron.*, vol. 13, no. 5, pp. 203–214, Oct. 2019.

[19] M. Usman, S. Althunibat, and K. Qaraqe, "Mobility dependent hybrid RF/FSO backhaul in UAV assisted cellular networks," in *Proc. IEEE 25th Int. Workshop Comput. Aided Modeling Design Commun. Links Netw. (CAMAD)*, Sep. 2020, pp. 1–6.

[20] Q. Sun, Z. Zhang, Y. Zhang, M. López-Benítez, and J. Zhang, "Performance analysis of dual-hop wireless systems over mixed FSO/RF fading channel," *IEEE Access*, vol. 9, pp. 85529–85542, 2021.

[21] E. Lee, J. Park, D. Han, and G. Yoon, "Performance analysis of the asymmetric dual-hop relay transmission with mixed RF/FSO links," *IEEE Photon. Technol. Lett.*, vol. 23, no. 21, pp. 1642–1644, Nov. 15, 2011.

[22] I. S. Ansari, F. Yilmaz, and M. Alouini, "Impact of pointing errors on the performance of mixed RF/FSO dual-hop transmission systems," *IEEE Wireless Commun. Lett.*, vol. 2, no. 3, pp. 351–354, Jun. 2013.

[23] E. Zedini, I. S. Ansari, and M.-S. Alouini, "Performance analysis of mixed Nakagami-m and gamma–gamma dual-hop FSO transmission systems," *IEEE Photon. J.*, vol. 7, no. 1, pp. 1–20, Dec. 2015.

[24] E. Zedini, H. Soury, and M. Alouini, "On the performance analysis of dual-hop mixed FSO/RF systems," *IEEE Trans. Wireless Commun.*, vol. 15, no. 5, pp. 3679–3689, May 2016.

[25] S. Anees and M. R. Bhatnagar, "Performance of an amplify-and-forward dual-hop asymmetric RF–FSO communication system," *J. Opt. Commun. Netw.*, vol. 7, no. 2, pp. 124–135, Feb. 2015.

[26] L. Yang, M. O. Hasna, and X. Gao, "Performance of mixed RF/FSO with variable gain over generalized atmospheric turbulence channels," *IEEE J. Sel. Areas Commun.*, vol. 33, no. 9, pp. 1913–1924, Sep. 2015.

[27] L. Kong, W. Xu, L. Hanzo, H. Zhang, and C. Zhao, "Performance of a free-space-optical relay-assisted hybrid RF/FSO system in generalized M-distributed channels," *IEEE Photon. J.*, vol. 7, no. 5, pp. 1–19, Aug. 2015.

[28] G. N. Kamga, S. Aïssa, T. R. Rasethuntsa, and M. Alouini, "Mixed RF/FSO communications with outdated-CSI-based relay selection under double generalized gamma turbulence, generalized pointing errors, and Nakagami-m fading," *IEEE Trans. Wireless Commun.*, vol. 20, no. 5, pp. 2761–2775, May 2021.

[29] E. Balti, M. Guizani, B. Hamdaoui, and B. Khalfi, "Aggregate hardware impairments over mixed RF/FSO relaying systems with outdated CSI," *IEEE Trans. Commun.*, vol. 66, no. 3, pp. 1110–1123, Mar. 2018.

[30] G. T. Djordjevic, M. I. Petkovic, A. M. Cvetkovic, and G. K. Karagiannidis, "Mixed RF/FSO relaying with outdated channel state information," *IEEE J. Sel. Areas Commun.*, vol. 33, no. 9, pp. 1935–1948, Sep. 2015.

[31] M. I. Petkovic, A. M. Cvetkovic, G. T. Djordjevic, and G. K. Karagiannidis, "Partial relay selection with outdated channel state estimation in mixed RF/FSO systems," *J. Lightw. Technol.*, vol. 33, no. 13, pp. 2860–2867, Jul. 1, 2015.

[32] E. Soleimani-Nasab and M. Uysal, "Generalized performance analysis of mixed RF/FSO cooperative systems," *IEEE Trans. Wireless Commun.*, vol. 15, no. 1, pp. 714–727, Jan. 2016.

[33] N. Varshney and A. K. Jagannatham, "Cognitive decode-and-forward MIMO-RF/FSO cooperative relay networks," *IEEE Commun. Lett.*, vol. 21, no. 4, pp. 893–896, Apr. 2017.

[34] S. Sharma, A. S. Madhukumar, and R. Swaminathan, "Switching-based cooperative decode-and-forward relaying for hybrid FSO/RF networks," *J. Opt. Commun. Netw.*, vol. 11, no. 6, pp. 267–281, Jun. 2019.

[35] E. Balti and M. Guizani, "Mixed RF/FSO cooperative relaying systems with co-channel interference," *IEEE Trans. Commun.*, vol. 66, no. 9, pp. 4014–4027, Sep. 2018.

[36] A. H. A. El-Malek, A. M. Salhab, S. A. Zummo, and M.-S. Alouini, "Effect of RF interference on the security-reliability tradeoff analysis of multiuser mixed RF/FSO relay networks with power allocation," *J. Lightw. Technol.*, vol. 35, no. 9, pp. 1490–1505, May 1, 2017.

[37] A. H. Abd El-Malek, A. M. Salhab, S. A. Zummo, and M. Alouini, "Security-reliability trade-off analysis for multiuser SIMO mixed RF/FSO relay networks with opportunistic user scheduling," *IEEE Trans. Wireless Commun.*, vol. 15, no. 9, pp. 5904–5918, Sep. 2016.

[38] N. I. Miridakis, M. Matthaiou, and G. K. Karagiannidis, "Multiuser relaying over mixed RF/FSO links," *IEEE Trans. Commun.*, vol. 62, no. 5, pp. 1634–1645, May 2014.
[39] N. H. Juel, A. S. M. Badrudduza, S. M. R. Islam, S. H. Islam, M. K. Kundu, I. S. Ansari, Md. M. Mowla, and K. Kwak, "Secrecy performance analysis of mixed α–μ and exponentiated Weibull RF-FSO cooperative relaying system," *IEEE Access*, vol. 9, pp. 72342–72356, 2021.
[40] X. Pan, H. Ran, G. Pan, Y. Xie, and J. Zhang, "On secrecy analysis of DF based dual hop mixed RF-FSO systems," *IEEE Access*, vol. 7, pp. 66725–66730, 2019.
[41] L. Yang, T. Liu, J. Chen, and M. Alouini, "Physical-layer security for mixed η–μ and $\mathcal{M}$-distribution dual-hop RF/FSO systems," *IEEE Trans. Veh. Technol.*, vol. 67, no. 12, pp. 12427–12431, Dec. 2018.
[42] A. Kumar and P. Garg, "Physical layer security for dual-hop FSO/RF system using generalized $\Gamma\Gamma/\eta - -\mu$ fading channels," *Int. J. Commun. Syst.*, vol. 31, no. 3, pp. 1–12, 2018.
[43] S. H. Islam, A. S. M. Badrudduza, S. M. R. Islam, F. I. Shahid, I. S. Ansari, M. K. Kundu, and H. Yu, "Impact of correlation and pointing error on secure outage performance over arbitrary correlated Nakagami-*m* and *M*-turbulent fading mixed RF-FSO channel," *IEEE Photon. J.*, vol. 13, no. 2, pp. 1–17, Mar. 2021.
[44] H. Lei, Z. Dai, I. S. Ansari, K. Park, G. Pan, and M. Alouini, "On secrecy performance of mixed RF-FSO systems," *IEEE Photon. J.*, vol. 9, no. 4, pp. 1–14, Aug. 2017.
[45] H. Lei, Z. Dai, K. Park, W. Lei, G. Pan, and M. Alouini, "Secrecy outage analysis of mixed RF-FSO downlink SWIPT systems," *IEEE Trans. Commun.*, vol. 66, no. 12, pp. 6384–6395, Dec. 2018.
[46] M. J. Saber, A. Keshavarz, J. Mazloum, A. M. Sazdar, and Md. J. Piran, "Physical-layer security analysis of mixed SIMO SWIPT RF and FSO fixed-gain relaying systems," *IEEE Syst. J.*, vol. 13, no. 3, pp. 2851–2858, Sep. 2019.
[47] Y. Ai, A. Mathur, M. Cheffena, M. R. Bhatnagar, and H. Lei, "Physical layer security of hybrid satellite-FSO cooperative systems," *IEEE Photon. J.*, vol. 11, no. 1, pp. 1–14, Feb. 2019.
[48] N. Varshney, A. K. Jagannatham, and P. K. Varshney, "Cognitive MIMO-RF/FSO cooperative relay communication with mobile nodes and imperfect channel state information," *IEEE Trans. Cognit. Commun. Netw.*, vol. 4, no. 3, pp. 544–555, Sep. 2018.
[49] H. Lei, H. Luo, K. Park, Z. Ren, G. Pan, and M. Alouini, "Secrecy outage analysis of mixed RF-FSO systems with channel imperfection," *IEEE Photon. J.*, vol. 10, no. 3, pp. 1–13, Jun. 2018.
[50] K. O. Odeyemi and P. A. Owolawi, "Physical layer security in mixed RF/FSO system under multiple eavesdroppers collusion and non-collusion," *Opt. Quantum Electron.*, vol. 50, no. 7, Jul. 2018.
[51] H. Lei, H. Luo, K. Park, I. S. Ansari, W. Lei, G. Pan, and M. Alouini, "On secure mixed RF-FSO systems with TAS and imperfect CSI," *IEEE Trans. Commun.*, vol. 68, no. 7, pp. 4461–4475, Jul. 2020.
[52] I. B. Djordjevic, "OAM-based hybrid free-space optical-terahertz multidimensional coded modulation and physical-layer security," *IEEE Photon. J.*, vol. 9, no. 4, pp. 1–12, Aug. 2017.
[53] Y. Ai, A. Mathur, H. Lei, M. Cheffena, and I. S. Ansari, "Secrecy enhancement of RF backhaul system with parallel FSO communication link," *Opt. Commun.*, vol. 475, Nov. 2020, Art. no. 126193.
[54] W. M. R. Shakir, "Physical layer security performance analysis of hybrid FSO/RF communication system," *IEEE Access*, vol. 9, pp. 18948–18961, 2021.
[55] K. O. Odeyemi, P. A. Owolawi, and O. O. Olakanmi, "Secrecy performance of cognitive underlay hybrid RF/FSO system under pointing errors and link blockage impairments," *Opt. Quantum Electron.*, vol. 52, no. 3, pp. 1–16, Mar. 2020.
[56] M. Kafafy, Y. Fahmy, M. Khairy, and M. Abdallah, "Secure backhauling over adaptive parallel mmWave/FSO link," in *Proc. IEEE Int. Conf. Commun. Workshops*, Jun. 2020, pp. 1–6.
[57] S. Althunibat, R. Mesleh, and K. Qaraqe, "Secure index-modulation based hybrid free space optical and millimeter wave links," *IEEE Trans. Veh. Technol.*, vol. 69, no. 6, pp. 6325–6332, Jun. 2020.
[58] D. R. Pattanayak, V. K. Dwivedi, and V. Karwal, "On the physical layer security of hybrid RF-FSO system in presence of multiple eavesdroppers and receiver diversity," *Opt. Commun.*, vol. 477, Dec. 2020, Art. no. 126334.
[59] S. Sharma, A. Madhukumar, and S. Ramabadran, "Performance optimisation for dual-hop hybrid FSO/RF system with selection combining," *IET Optoelectron.*, vol. 14, no. 6, pp. 422–433, Dec. 2020.
[60] A. Tahami, A. Dargahi, K. Abedi, and A. Chaman-Motlagh, "A new relay based architecture in hybrid RF/FSO system," *Phys. Commun.*, vol. 36, Oct. 2019, Art. no. 100818.
[61] M. A. Amirabadi and V. T. Vakili, "Performance comparison of two novel relay-assisted hybrid FSO/RF communication systems," *IET Commun.*, vol. 13, no. 11, pp. 1551–1556, Jul. 2019.
[62] Md. Z. Hassan, Md. J. Hossain, J. Cheng, and V. C. M. Leung, "Hybrid RF/FSO backhaul networks with statistical-QoS-aware buffer-aided relaying," *IEEE Trans. Wireless Commun.*, vol. 19, no. 3, pp. 1464–1483, Mar. 2020.
[63] M. Najafi, V. Jamali, and R. Schober, "Optimal relay selection for the parallel hybrid RF/FSO relay channel: Non-buffer-aided and buffer-aided designs," *IEEE Trans. Commun.*, vol. 65, no. 7, pp. 2794–2810, Jul. 2017.
[64] S. C. Tokgoz, S. Althunibat, S. L. Miller, and K. A. Qaraqe, "Outage analysis of relay-based dual-hop hybrid FSO-mmWave systems," *IEEE Access*, vol. 10, pp. 2895–2907, 2022.
[65] S. C. Tokgoz, S. Althunibat, S. L. Miller, and K. A. Qaraqe, "On the secrecy capacity of hybrid FSO-mmWave wiretap channels," *IEEE Trans. Veh. Technol.*, vol. 71, no. 4, pp. 4073–4086, Apr. 2022.
[66] S. C. Tokgoz, S. Althunibat, S. L. Miller, and K. A. Qaraqe, "On the secrecy capacity of hybrid FSO-mmWave links with correlated wiretap channels," *Opt. Commun.*, vol. 499, Nov. 2021, Art. no. 127252.
[67] A. D. Wyner, "The wire-tap channel," *Bell Syst. Tech. J.*, vol. 54, no. 8, pp. 1355–1387, Oct. 1975.
[68] A. K. Majumdar, "Free-space laser communication performance in the atmospheric channel," *J. Opt. Fiber Commun. Rep.*, vol. 2, no. 4, pp. 345–396, Oct. 2005.
[69] L. C. Andrews, R. L. Phillips, and C. Y. Hopen, *Laser Beam Scintillation With Applications*, vol. 99, 2nd ed. Bellingham, WA, USA: SPIE Press, 2001.
[70] T. S. Rappaport, S. Sun, R. Mayzus, H. Zhao, Y. Azar, K. Wang, G. N. Wong, J. K. Schulz, M. Samimi, and F. Gutierrez, "Millimeter wave mobile communications for 5G cellular: It will work!" *IEEE Access*, vol. 1, pp. 335–349, 2013.
[71] A. I. Sulyman, A. T. Nassar, M. K. Samimi, G. R. Maccartney, T. S. Rappaport, and A. Alsanie, "Radio propagation path loss models for 5G cellular networks in the 28 GHz and 38 GHz millimeter-wave bands," *IEEE Commun. Mag.*, vol. 52, no. 9, pp. 78–86, Sep. 2014.
[72] S. Hur, S. Baek, B. Kim, Y. Chang, A. F. Molisch, T. S. Rappaport, K. Haneda, and J. Park, "Proposal on millimeter-wave channel modeling for 5G cellular system," *IEEE J. Sel. Topics Signal Process.*, vol. 10, no. 3, pp. 454–469, Apr. 2016.
[73] *Study on Channel Model for Frequencies From 0.5 to 100 GHz (Release 15)*, 3GPP Radio Access Network Working Group, document TR 38.901, 2018. [Online]. Available: https://www.etsi.org/deliver/etsi_tr/138900_138999/138901/14.03.00_60/tr_138901v140300p.pdf
[74] J. G. Andrews, T. Bai, M. N. Kulkarni, A. Alkhateeb, A. K. Gupta, and R. W. Heath Jr., "Modeling and analyzing millimeter wave cellular systems," *IEEE Trans. Commun.*, vol. 65, no. 1, pp. 403–430, Jan. 2017.
[75] M. K. Simon and M.-S. Alouini, *Digital Communication Over Fading Channels*, vol. 95, 2nd ed. Hoboken, NJ, USA: Wiley, 2005.
[76] I. Gradshteyn and I. Ryzhik, *Table of Integrals, Series, and Products*, 7th ed. New York, NY, USA: Academic, 2014.
[77] A. Prudnikov, Y. A. Brychkov, and O. Marichev, *Integrals and Series, Volume 3: More Special Functions*, 1st ed. New York, NY, USA: New York Gordon and Breach Science Publishers, 1986.
[78] M. O. Hasna and M.-S. Alouini, "A performance study of dual-hop transmissions with fixed gain relays," *IEEE Trans. Wireless Commun.*, vol. 3, no. 6, pp. 1963–1968, Nov. 2004.
[79] A. Bletsas, A. Khisti, D. P. Reed, and A. Lippman, "A simple cooperative diversity method based on network path selection," *IEEE J. Sel. Areas Commun.*, vol. 24, no. 3, pp. 659–672, Mar. 2006.
[80] S. Ikki and M. Ahmed, "Performance analysis of cooperative diversity wireless networks over Nakagami-*m* fading channel," *IEEE Commun. Lett.*, vol. 11, no. 4, pp. 334–336, Apr. 2007.
[81] H. Suraweera, R. Louie, Y. Li, G. Karagiannidis, and B. Vucetic, "Two hop amplify-and-forward transmission in mixed Rayleigh and Rician fading channels," *IEEE Commun. Lett.*, vol. 13, no. 4, pp. 227–229, Apr. 2009.
[82] A. Prudnikov, Y. A. Brychkov, and O. Marichev, *Integrals and Series, Volume 1: Elementary Functions*, 4th ed. New York, NY, USA: New York Gordon and Breach Science Publishers, 1998.
[83] V. S. Adamchik and O. I. Marichev, "The algorithm for calculating integrals of hypergeometric type functions and its realization in REDUCE system," in *Proc. Int. Symp. Symbolic Algebr. Comput.*, Jul. 1990, pp. 212–224.

[84] S. H. Islam, A. S. M. Badrudduza, S. M. Riazul Islam, F. I. Shahid, I. S. Ansari, M. K. Kundu, S. K. Ghosh, M. B. Hossain, A. S. M. S. Hosen, and G. H. Cho, "On secrecy performance of mixed generalized gamma and Málaga RF-FSO variable gain relaying channel," *IEEE Access*, vol. 8, pp. 104127–104138, 2020.
[85] H. Lei, C. Gao, I. S. Ansari, Y. Guo, G. Pan, and K. A. Qaraqe, "On physical-layer security over SIMO generalized-K fading channels," *IEEE Trans. Veh. Technol.*, vol. 65, no. 9, pp. 7780–7785, Sep. 2016.
[86] I. I. Kim, B. McArthur, and E. J. Korevaar, "Comparison of laser beam propagation at 785 nm and 1550 nm in fog and haze for optical wireless communications," *Proc. SPIE*, vol. 4214, pp. 26–37, Feb. 2001.
[87] H. Chergui, M. Benjillali, and S. Saoudi, "Performance analysis of project-and-forward relaying in mixed MIMO-pinhole and Rayleigh dual-hop channel," *IEEE Commun. Lett.*, vol. 20, no. 3, pp. 610–613, Mar. 2016.

SAUD ALTHUNIBAT (Senior Member, IEEE) received the Ph.D. degree in telecommunications from the University of Trento, Trento, Italy, in 2014. He is currently an Associate Professor with Al-Hussein Bin Talal University, Ma'an, Jordan. He is coordinating several funded projects, including IREEDER (EU-Erasmus-Plus), PHY-SEC (NATO-SPS), and RESCUE (NATO-SPS). He has authored more than 150 scientific articles. His research interests include wireless communication topics, such as index modulation, spectrum sharing, cognitive radio, wireless sensor networks, energy efficiency, and resource allocation. He was a recipient of the Best Paper Award from IEEE CAMAD 2012 and IEEE GLOBECOM 2022. He was a recipient of the Distinguished Researcher Award granted by the Hamdi Mango Center, The University of Jordan, in 2022. He is the General Co-Chair of the BROADNETs 2018 Conference. He was selected as an Exemplary Reviewer of the IEEE COMMUNICATION LETTERS, in 2013.

SEZER C. TOKGOZ (Member, IEEE) was born in Istanbul, Turkey, in 1994. He received the B.S. degree in electrical and electronics engineering from Istanbul Commerce University, in July 2017, the M.S. degree in electrical and electronics engineering from the University of Istanbul, in January 2019, the M.S. degree in electrical and telecommunications engineering from Istanbul Commerce University, in February 2019, and the Ph.D. degree in electrical engineering from Texas A&M University, College Station, TX, USA, in December 2022. He is currently a Senior Engineer with WR&D, Qualcomm Technologies Inc. His current research interests include 5G and beyond radio access technologies, physical layer security, multi-carrier wireless systems, wireless propagation channel measurement and modeling, and millimeter wave and optical communications.

SERHAN YARKAN (Senior Member, IEEE) received the B.S. and M.Sc. degrees in computer science from Istanbul University, Istanbul, Turkey, in 2001 and 2003, respectively, and the Ph.D. degree from the University of South Florida, Tampa, FL, USA, in 2009. From 2010 to 2012, he was a Postdoctoral Research Associate with the Department of Computer and Electrical Engineering, Texas A&M University, College Station, TX, USA. He is currently an Associate Professor with the Department of Electrical and Electronics Engineering, Istanbul Commerce University, Istanbul. His current research interests include statistical signal processing, cognitive radio, wireless propagation channel measurement and modeling, cross-layer adaptation and optimization, interference management in next-generation wireless networks, and underground mine channels and disaster communications.

SCOTT L. MILLER was born in Los Angeles, CA, USA, in 1963. He received the B.S., M.S., and Ph.D. degrees in electrical engineering from the University of California at San Diego (UCSD), in 1985, 1986, and 1988, respectively. He has also held visiting positions at Motorola Inc., The University of Utah, and UCSD. He joined the Department of Electrical and Computer Engineering, University of Florida, where he was an Assistant Professor, from 1988 to 1993, and an Associate Professor, from 1993 to 1998. In August 1998, he joined the Electrical and Computer Engineering Department, Texas A&M University, where he is currently the Debbie and Dennis Segers'75 Professor and an Associate Dean for Graduate Programs with the Dwight Look College of Engineering. He has taught courses at both the graduate and undergraduate levels on topics, such as linear circuits, signals and systems, engineering mathematics, digital and analog communications, probability and random processes, coding, information theory, spread spectrum, detection and estimation theory, wireless communications, signal processing, queuing theory, and communication networks. He has published over 75 refereed journals and conference papers on a variety of topics in the area of digital communication theory. His current research interests include wireless communications and signal processing. He is the past Chair of the IEEE Communications Theory Technical Committee.

KHALID A. QARAQE (Senior Member, IEEE) was born in Bethlehem. He received the B.S. degree (Hons.) in electrical engineering from the University of Technology, Bagdad, Iraq, in 1986, the M.S. degree in electrical engineering from The University of Jordan, Amman, Jordan, in 1989, and the Ph.D. degree in electrical engineering from Texas A&M University, College Station, TX, USA, in 1997.

From 1989 to 2004, he held a variety of positions in many companies. He has over 12 years of experience in the telecommunication industry. He has worked on numerous projects and has experience in product development, design, deployments, testing, and integration. He joined the Department of Electrical and Computer Engineering, Texas A&M University at Qatar, in July 2004, where he is currently a Professor and the Managing Director of the Center for Remote Healthcare Technology, Qatar. He received more than 20 research projects consisting of more than U.S. $13M from local industries in Qatar and the Qatar National Research Foundation (QNRF). He has published more than 131 journal articles in top IEEE journals. He has published and presented 250 papers at prestigious international conferences. He has 20 book chapters published and four books and presented several tutorials and talks. He holds three patents. His research interests include communication theory and its application to design and performance, analysis of cellular systems, indoor communication systems, mobile networks, broadband wireless access, cooperative networks, cognitive radio, diversity techniques, index modulation, visible light communication, FSO, telehealth, and noninvasive biosensors.

Dr. Qaraqe received the Itochu Professorship Award (2013–2015), the Best Researcher Award from QNRF, in 2013, the Best Paper Award from the IEEE First Workshop on Smart Grid and Renewable Energy, in 2015, the Best Paper Award from the IEEE GLOBECOM 2014, the Best Poster Award from the IEEE Dyspan Conference, in 2012, the TAMUQ Research Excellence Award, in 2010, the Best Paper Award from ComNet, in 2010, the Best Paper Award from CROWNCOM, in 2009, the Best Paper Award from the ICSPC'0, in 2007, the *IEEE Signal Processing Magazine* Best Column Award, in 2018, the Best Oral Presentation Award from CECNet 2018, the Best Paper Award from the Green Communications, Computing and Technologies Conference, in 2016, the Faculty of the Year (Student Award), in 2016 and 2015, respectively, and the Best Faculty Award by the Student Body, in 2015.